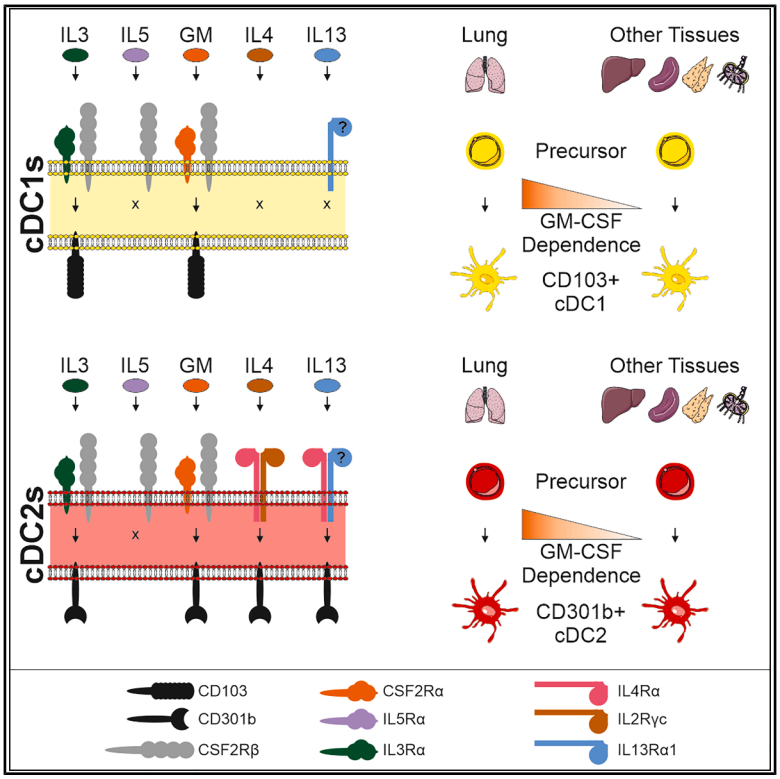
Cell Reports

Article

GM-CSF and specific type 2 cytokines induce CD103$^+$ and CD301b$^+$ cell states in cDC1s and cDC2s

Graphical abstract



Highlights

- CD103 and CD301b mark cytokine-induced states within cDC1s and cDC2s, respectively
- Pre-committed DC2 and DC3 progenitors give rise to CD301b$^+$ DCs
- CD103 and CD301b expression is driven by GM-CSF and specific type 2 cytokines
- Lung DCs selectively require GM-CSF sensing to acquire these functional states

Authors

Lukas Amon, Damir Vurnek, Anna Seichter, ..., Bart N. Lambrecht, Christian H.K. Lehmann, Diana Dudziak

Correspondence

lukas.amon@irc.vib-ugent.be (L.A.), diana.dudziak@med.uni-jena.de (D.D.)

In brief

Amon et al. show that GM-CSF and specific type 2 cytokines induce functional states in cDC1s and cDC2s, marked by CD103 and CD301b. In the lung, DC-intrinsic GM-CSF sensing is indispensable for acquisition of these states.

Amon et al., 2025, Cell Reports *44*, 116589
December 23, 2025 © 2025 The Authors. Published by Elsevier Inc.
https://doi.org/10.1016/j.celrep.2025.116589

CellPress

Cell Reports

CellPress
OPEN ACCESS

Article

GM-CSF and specific type 2 cytokines induce CD103$^+$ and CD301b$^+$ cell states in cDC1s and cDC2s

Lukas Amon,[1,2,3,*] Damir Vurnek,[4] Anna Seichter,[1] Giorgi Tchitashvili,[1] Tomasz Kaszubowski,[1] Markus Mroz,[5] Nincy Debeuf,[2,3] Tina Vogler,[6] Nicole Küpper,[7] Kaushikk Ravi Rengarajan,[8] Lukas Lächele,[1] Nounagnon R. Tochoedo,[4] Anna Baranska,[1,21] Stella E. Autenrieth,[9] Falk Nimmerjahn,[10,11] Kai Hildner,[6,12] Klaus Pfeffer,[7] Barbara U. Schraml,[8] Lukas Heger,[1,13] Bart N. Lambrecht,[2,3,14] Christian H.K. Lehmann,[1,11,12,15] and Diana Dudziak[1,4,16,17,18,19,20,22,*]

[1]Laboratory of Dendritic Cell Biology, Department of Dermatology, University Hospital Erlangen, Friedrich-Alexander-University of Erlangen-Nürnberg, 91052 Erlangen, Germany
[2]Laboratory of Immunoregulation and Mucosal Immunology, VIB Center for Inflammation Research, 9052 Ghent, Belgium
[3]Department of Internal Medicine and Pediatrics, Ghent University, 9000 Ghent, Belgium
[4]Institute of Immunology, Jena University Hospital, Friedrich Schiller University Jena, 07743 Jena, Germany
[5]Core Unit Cell Sorting and Immunomonitoring, Friedrich-Alexander-University Erlangen-Nürnberg, 91054 Erlangen, Germany
[6]Department of Medicine 1, University Hospital Erlangen, Friedrich-Alexander-University Erlangen-Nürnberg, Erlangen, Germany
[7]Institute of Medical Microbiology and Hospital Hygiene, Heinrich Heine University Düsseldorf, Düsseldorf, Germany
[8]Institute for Immunology, Biomedical Center Munich, Faculty of Medicine, Ludwig-Maximilians-Universität in Munich, 82152 Planegg-Martinsried, Germany
[9]Research Group "Dendritic Cells in Infection and Cancer" (D431), German Cancer Research Center (Deutsches Krebsforschungszentrum), 69120 Heidelberg, Germany
[10]Division of Genetics, Department of Biology, Friedrich-Alexander-University Erlangen-Nürnberg, 91058 Erlangen, Germany
[11]FAU Profile Center Immunomedicine (FAU I-MED), 91054 Erlangen, Germany
[12]Deutsches Zentrum Immuntherapie (DZI), 91054 Erlangen, Germany
[13]Department of Transfusion Medicine and Haemostaseology, University Hospital Erlangen, Friedrich-Alexander University of Erlangen-Nürnberg, 91054 Erlangen, Germany
[14]Department of Pulmonary Medicine, Erasmus University Medical Center Rotterdam, 3015 Rotterdam, the Netherlands
[15]Department of Pediatrics and Adolescent Medicine, Friedrich-Alexander-University Erlangen-Nürnberg, 91054 Erlangen, Germany
[16]Cluster of Excellence Balance of the Microverse, Friedrich Schiller University Jena, 07743 Jena, Germany
[17]Center for Sepsis Control and Care, Jena University Hospital, 07747 Jena, Germany
[18]Zentrum für Alternsforschung Jena (ZAJ), Jena, Germany
[19]Comprehensive Cancer Center Central Germany (CCCG), 07743 Jena, Germany
[20]Core Facility Cytometry, Jena University Hospital, 07743 Jena, Germany
[21]Present address: Miltenyi Biotec B.V. & Co. KG, Friedrich-Ebert-Straße 68, Bergisch, 51429 Gladbach, Germany
[22]Lead contact
*Correspondence: lukas.amon@irc.vib-ugent.be (L.A.), diana.dudziak@med.uni-jena.de (D.D.)
https://doi.org/10.1016/j.celrep.2025.116589

SUMMARY

The heterogeneity of conventional dendritic cells type 1 (cDC1s) and type 2 (cDC2s) is well established, yet the identity and origin of CD301b$^+$ cDC2s remain debated. Here, we show that CD301b$^+$ cDC2s and CD103$^+$ cDC1s develop from pre-committed progenitors in response to granulocyte/macrophage colony-stimulating factor (GM-CSF). While CD103$^+$ cDC1s acquire their phenotype and functional properties through GM-CSF-driven differentiation from pre-cDC1s, CD301b$^+$ cDC2s emerge as cytokine-induced states from DC2- and DC3-committed progenitors. CD103$^+$ cDC1s and CD301b$^+$ cDC2s exhibit enhanced T cell priming capacities and distinct cytokine expression profiles upon GM-CSF exposure. *In vivo*, DC-intrinsic GM-CSF sensing is dispensable for acquiring CD103 and CD301b expression with the notable exception of lung DCs, while specific type 2 cytokines induce CD103 and CD301b *ex vivo*. These findings identify GM-CSF and specific type 2 cytokines as central regulators of cDC1 and cDC2 effector differentiation and establish CD301b as a marker of a cytokine-driven cDC2 state.

INTRODUCTION

Conventional dendritic cells (cDCs) represent central orchestrators of immune responses. cDCs were classified based on ontogeny, phenotype, and function into cDC1s and cDC2s across murine and human tissues.[1] They arise from hematopoietic stem cells (HSCs) located in bone marrow. Upon development of HSCs via multi-potent progenitors (MPPs) into common myeloid progenitors (CMPs), CMPs bifurcate into granulocyte-macrophage progenitors (GMPs) and monocyte-dendritic cell

This is an open access article under the CC BY license (http://creativecommons.org/licenses/by/4.0/).

progenitors (MDPs).[2–4] GMPs further develop into granulocyte progenitors (GPs), giving rise to granulocytes and the predecessor of monocytes termed common monocyte progenitor (cMoP).[2–4] Meanwhile, MDPs develop via Clec9A-expressing cDC-committed common DC precursors (CDPs) into pre-cDC1s and pre-cDC2s.[3,5,6] While the majority of DC lineage development occurs in the bone marrow, pre-cDCs traverse via the bloodstream to their target tissues, where they turn into cDCs.[5]

All mouse cDCs require FLT3-ligand recognized by fms-like tyrosine kinase 3 (CD135; FLT3) for their development.[7,8] Further, they express major histocompatibility complex class II (MHC-II), CD11c, and CD26 across tissues.[9] cDC1s are marked by XC motif chemokine receptor 1 (XCR1), CD103 (peripheral tissues), CD8α (lymphoid tissues), CD370 (Clec9A), CD272 (BTLA), and cell adhesion molecule 1 (CADM1, NECL-2).[2,6,10–14] Functionally, cDC1s are prime inducers of cytotoxic $CD8^+$ T cell responses by cross-presentation of extracellular antigens and drive T helper cell type 1 (T_H1) responses mediated via their superior interleukin12 (IL12) production in mice.[15–26] The fate, maintenance, and functions of cDC1s are regulated by a complex transcription factor network, including interferon regulatory factor 8 (IRF8), inhibitor of DNA binding 2 (ID2), dendritic cell-specific transcript (DC-SCRIPT), nuclear factor, interleukin 3 regulated (NFIL-3), ETS variant transcription factor 6 (ETV6), and basic leucine zipper ATF-like transcription factor 3 (BATF3).[2,27–32] Contrarily, cDC2s are $CD172a^+$[9,11] and specialized for inducing T_H2 and T_H17 responses directed against extracellular bacteria and fungi.[31,33–39] The superior ability of cDC2s for $CD4^+$ T cell priming is reflected by their antigen presentation machinery specialized for presentation via MHC-II molecules.[18] While the transcription factor zinc finger e-box binding homeobox 2 (ZEB2) is critical for cDC2 lineage specification, multiple transcription factors contribute to the regulation of cDC2 maintenance, function, and the development of functionally distinct cDC2 subpopulations, including IRF4, TNF receptor associated factor 6 (TRAF6), RELB, IRF2, Krüppel-like factor 4 (KLF4), and neurogenic locus notch homolog protein 2/recombination signaling binding protein for immunoglobulin kappa J region (NOTCH2/RBPJ).[2,31,36,38–43]

The development of sophisticated mouse models for myeloid cell annotation and DC analysis and the advent of single-cell omics revealed a high heterogeneity within cDC2s leading to the classification of endothelial cell-selective adhesion Mmlecule (ESAM)$^+$T-bet$^+$CD4$^+$CD11b^{low} cDC2As with a dual dependence on lymphotoxin-beta (LTβ) and NOTCH2/RBPJ and KLF4-dependent Clec12A$^+$T-bet$^-$CD4$^-$CD11b^{high} cDC2Bs.[11,36,37,39,41,44–54] This dichotomy is already established within the bone marrow.[47,50] Functionally, cDC2As drive T_H17 cell responses, whereas cDC2Bs induce T_H2 T cell responses.[36,37,39] Following the discovery of a plasmacytoid DC (pDC)-like cell population in murine spleen with transcriptional resemblance to cDC2s, pDC-like cells of lymphoid origin were identified as bona fide cDC2 precursors existing in parallel to classical pre-cDC2s.[49,50,55–58] These Siglec-H$^+$ pDC-like cells preferentially gave rise to cDC2As, whereas Siglec-H$^-$ pre-cDC2s preferentially developed into cDC2Bs.[47,58,59] In addition to the dichotomy of cDC2As and cDC2Bs, CD301b marks a fraction of cDC2s key for T_H2 and T_H17 responses.[33–35,39] These CD301b$^+$ cDC2s particularly arise in barrier tissues in response to granulocyte/macrophage colony-stimulating factor (GM-CSF).[33–35,39] On top, murine splenic cDC2s previously summarized phenotypically as XCR1$^-$CD172a$^+$ were found to consist of two ontogenetically distinct populations. These XCR1$^-$CD172a$^+$ cDC2s contained FcγRIIB/III$^-$ or FcγRIIB/III$^+$ cells, termed DC2s and DC3s, respectively.[11,50,60] While FcγRIIB/III$^-$ DC2s follow a classical DC developmental trajectory originating from CDPs and pre-cDC2s, FcγRIIB/III$^+$ DC3s have been suggested to arise from a Ly6C$^+$ fraction of MDPs via pro-DC3s.[50,60]

We showed that ESAM-based heterogeneity is spleen specific, while Clec12A, CD301b, and FcγRIIB/III delineate conserved cDC2 diversity across tissues.[11,12] However, whether CD301b$^+$ cDC2s constitute a separate developmental lineage or reflect a GM-CSF-driven cellular state remains unresolved.

Here, we demonstrate that CD301b$^+$ cDC2s are bona fide DCs developing from pre-cDC2s and pro-DC3s *ex vivo* in response to FLT3L and GM-CSF. Similarly, GM-CSF induces CD103 on developing cDC1s. Functionally, GM-CSF broadly boosts DC subset functions in response to diverse TLR ligands including T cell priming and cytokine production. Under homeostatic conditions, CD301b and CD103 expression requires DC-intrinsic GM-CSF sensing specifically in the lung, while type 2 cytokines such as IL3, IL4, and IL13 can phenocopy the actions of GM-CSF *ex vivo*. Together, these findings redefine CD301b$^+$ cDC2s as a cytokine-induced cellular state shared across FcγRIIB/III$^-$ DC2s and FcγRIIB/III$^+$ DC3s, highlighting GM-CSF and type 2 cytokines as a central regulator of functional differentiation in cDC1s and cDC2s.

RESULTS

GM-CSF drives the generation of phenotypically distinct CD301b$^+$ cDC2s and CD103$^+$ cDC1s

To mirror the heterogeneity of DCs *in vivo*, we first established an *in vitro* culture protocol to generate high numbers of CD301b$^+$ cDC2s and CD103$^+$ cDC1s, which were described to arise in culture systems containing GM-CSF.[34,61,62] After facilitating DC generation via FLT3L, GM-CSF was supplied to cultures after 4 days, followed by flow cytometric analysis after 6 days (Figures 1A and S1A). While cDC (DAPI$^-$CD3ε$^-$CD19$^-$NK1.1$^-$B220$^-$Siglec-H$^-$Ly6C$^-$CD88$^-$MHCII$^+$CD11c$^+$) development was dependent on FLT3L, CD301b$^+$ cDC2s were exclusively detected within GM-CSF-containing cultures, highlighting GM-CSF as driving force for CD301b$^+$ differentiation (Figures 1B and 1C). Further, GM-CSF induced a CD103$^+$ phenotype in all XCR1$^+$ cDC1s (Figures 1B and 1C). Independent of GM-CSF availability, cDC1s were CD8α$^-$ post-differentiation, while cDC2s were ESAM$^-$ (Figures 1B and 1E).

To validate subset identity, we cross-compared the phenotype of differentiated DCs to their splenic counterparts. Therefore, CD11c-enriched splenic DCs and differentiated DCs (day 6) were stained with a shared antibody backbone, analyzed via flow cytometry, and cross-compared within a uniform manifold approximation and projection (UMAP) (Figure 1D). This revealed

CellPress
OPEN ACCESS

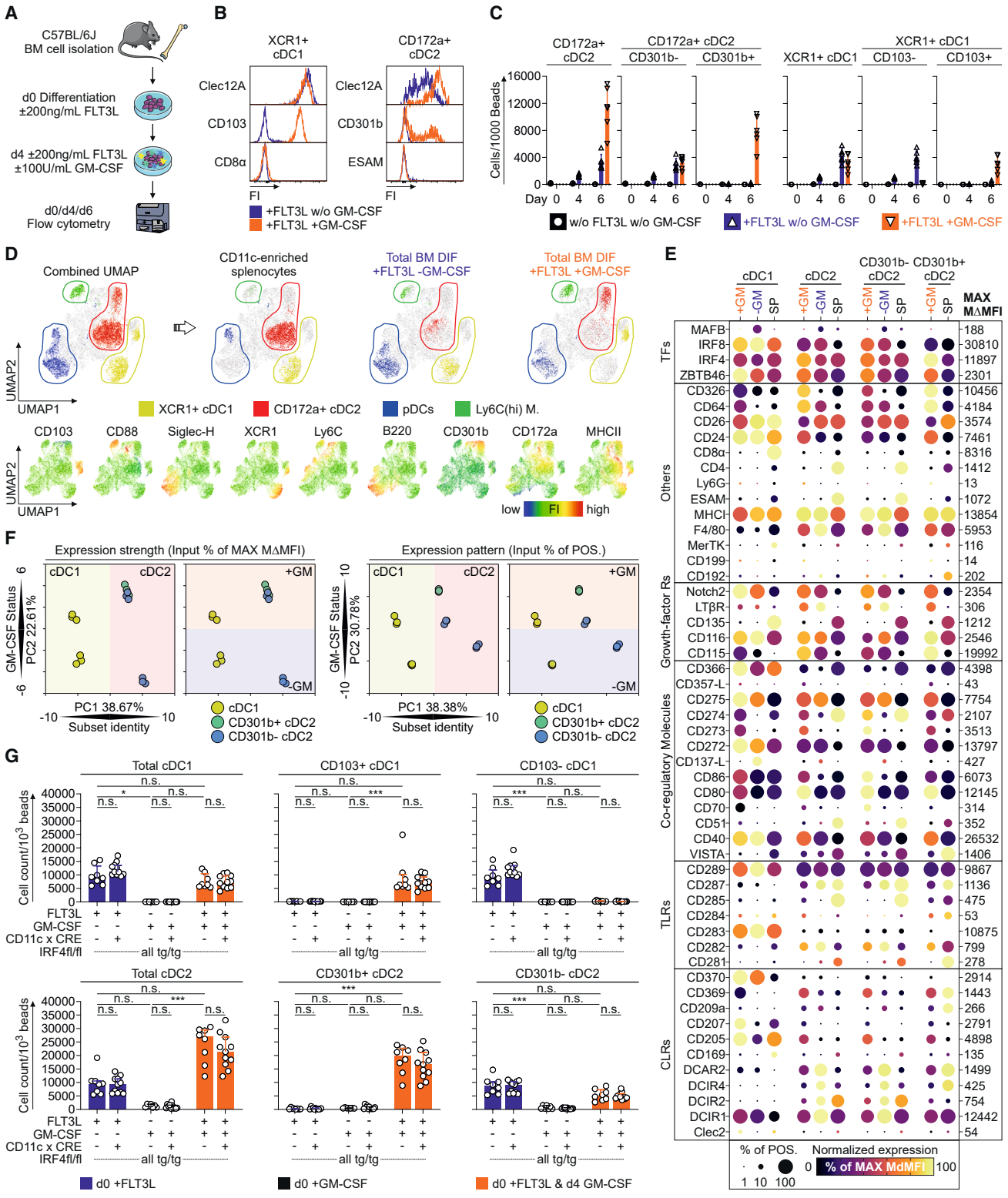


Figure 1. GM-CSF drives the generation of bona fide FLT3L-dependent CD301b$^+$ cDC2 and CD103$^+$ cDC1

(A) Workflow of cDC differentiation.

(B) Representative marker histograms (d6).

(C) Kinetics of DC subset output during differentiation. *n* = 6 biological replicas/condition. DC output was quantified with precision count beads. Mean ± SD.

(legend continued on next page)

that generated monocytes and pDCs formed superclusters with their *in vivo* counterparts that were distinct from cDCs. Further, cDC2s cultured ± GM-CSF resembled CD301b$^+$ or CD301b$^-$ splenic cDC2s, respectively. Finally, cDC1s generated without GM-CSF aligned with splenic cDC1s, whereas GM-CSF-cultured CD103$^+$ cDC1s formed a novel cluster.

Bone marrow cultures solely based on GM-CSF facilitate the generation of MerTK$^+$ macrophages outnumbering produced DCs.[63] To assess, if generated DCs resemble a bona fide DC phenotype distinct from macrophages, we compiled a protein library via flow cytometry containing canonical myeloid-associated molecules (Figure 1E). All DCs generated in the presence or absence of GM-CSF *in vitro* were lacking macrophage markers (MafB/MerTK/VISTA/CD51/CD88), whereas cDC markers (Zbtb46/CD26/MHC-II) were highly expressed (Figures 1D and 1E).[9,11,51,54] Further, differentiated cDC1s (CD205/CD207/CD370/CD283/CD272/CD366/CD24/IRF8) and cDC2s (IRF4/CD172a) aligned with their *in vivo* counterparts (Figures 1D and 1E).[11] Finally, all cDC subsets expressed toll-like receptor 9 (TLR9, CD289), rendering its stimulation via ODN1826 (cytosine-phosphate-guanine [CpG]) as an attractive strategy to cross-compare functionality of generated DC subsets under inflammatory conditions.

To understand the underlying factors regulating protein expression within differentiated DCs, principal component analyses (PCA) with the data displayed in Figure 1E were performed. As input, either the expression pattern (percentage of positive cells over isotype control/fluorescence minus one [FMO]) or expression strength (percentage of maximum meanΔmean fluorescence intensity [MFI]) was utilized (Figure 1F). The PCA revealed a dominant principal component (PC) 1 and a subdominant PC2 together explaining the majority of variance within the dataset. Independent on the input parameter, subset identity (cDC1 vs. cDC2), and thus ontogeny, separated cells along PC1. Contrarily, the use of GM-CSF during cultures separated the subsets along PC2. Thus, GM-CSF modulated the primarily cell-identity-driven proteome.

Previously, FLT3L was determined as essential for DC development.[7] Further, GM-CSF is thought to regulate multiple aspects of macrophages and monocytes via IRF4, which showed peak expression within GM-CSF-differentiated CD301b$^+$ cDC2s (Figure 1E).[64] To understand the developmental requirements, we performed DC differentiation employing bone marrow isolated from CD11c^{CRE}xIRF4$^{fl/fl}$ mice with either FLT3L (d0), GM-CSF (d0), or FLT3L (d0) and GM-CSF (d4). Our results revealed that FLT3L was a prerequisite for general cDC1 and cDC2 development, which completely failed in cultures containing GM-CSF alone (Figure 1G). However, differentiation of CD103$^+$ cDC1s and CD301b$^+$ cDC2s was dependent on the dual presence of GM-CSF and FLT3L. Finally, conditional deletion of IRF4 in CD11c$^+$ cells had no impact on the development of any cDC2 subset.

In summary, the developed *in vitro* culture system led to the generation of bona fide FLT3L-dependent DCs that were distinct from other myeloid lineages.

GM-CSF modulates and boosts functional features of cDCs

To understand, if generated CD301b$^+$ cDC2s and CD103$^+$ cDC1s display functional differences in comparison to their CD301b$^-$ and CD103$^-$ counterparts, we investigated their secreted cytokine/chemokine profiles in reaction to a variety of infection mimics (Figures 2A, 2B, S1B, and S1C). Our results revealed that profiles of FLT3L + GM-CSF-differentiated cDCs strongly differed from their FLT3L-differentiated counterparts upon TLR-ligand stimulation (Figure 2B). While GM-CSF during differentiation attenuated CCL3 and CCL4 secretion by cDC1s and CD301b$^-$ cDC2s, it boosted the production of IL-12p40, CCL5, and CCL22 in CD103$^+$ cDC1s after Zymosan and CD301b$^+$ cDC2s after ODN1826 stimulation, respectively. Thus, GM-CSF differentiated CD301b$^+$ cDC2s produce a cytokine/chemokine profile distinct from other cDC2s.

Further, we analyzed the impact of GM-CSF during differentiation on the expression of classical co-stimulatory molecules involved in T cell priming revealing that GM-CSF induced upregulation of CD70, CD80, and CD86 on cDC subsets (Figure 2C). Moreover, GM-CSF had an additive effect on co-stimulatory molecule expression upon ODN1826 stimulation.

To investigate, if CD301b$^+$ cDC2s are capable of T cell priming (Figures 2D and S2A), we co-cultured cDC subsets with ovalbumin (OVA)$_{257-264}$-specific CD8$^+$ T cells in the presence or absence of OVA$_{257-264}$ peptide (Figure 2E). We found that all GM-CSF-differentiated cDC subsets were superior in inducing T cell proliferation (Figure 2E). Since experimental settings based on the external loading of MHC molecules with peptides do not address subset-intrinsic capabilities for antigen uptake, processing, and presentation, sorted cDC subsets were additionally co-cultured with OVA$_{257-264}$-specific CD8$^+$ T cells, soluble ovalbumin (sOVA), and the TLR9 ligand ODN1826 (Figure 2F). While successful T cell priming was dependent on DC activation

(D) UMAP incorporating 7,500 cells per condition containing single, live, LIN$^-$ cells of bone marrow differentiation cultures +FLT3L ± GM-CSF (d6) and CD11c-enriched splenocytes. Displayed markers were used for clustering.

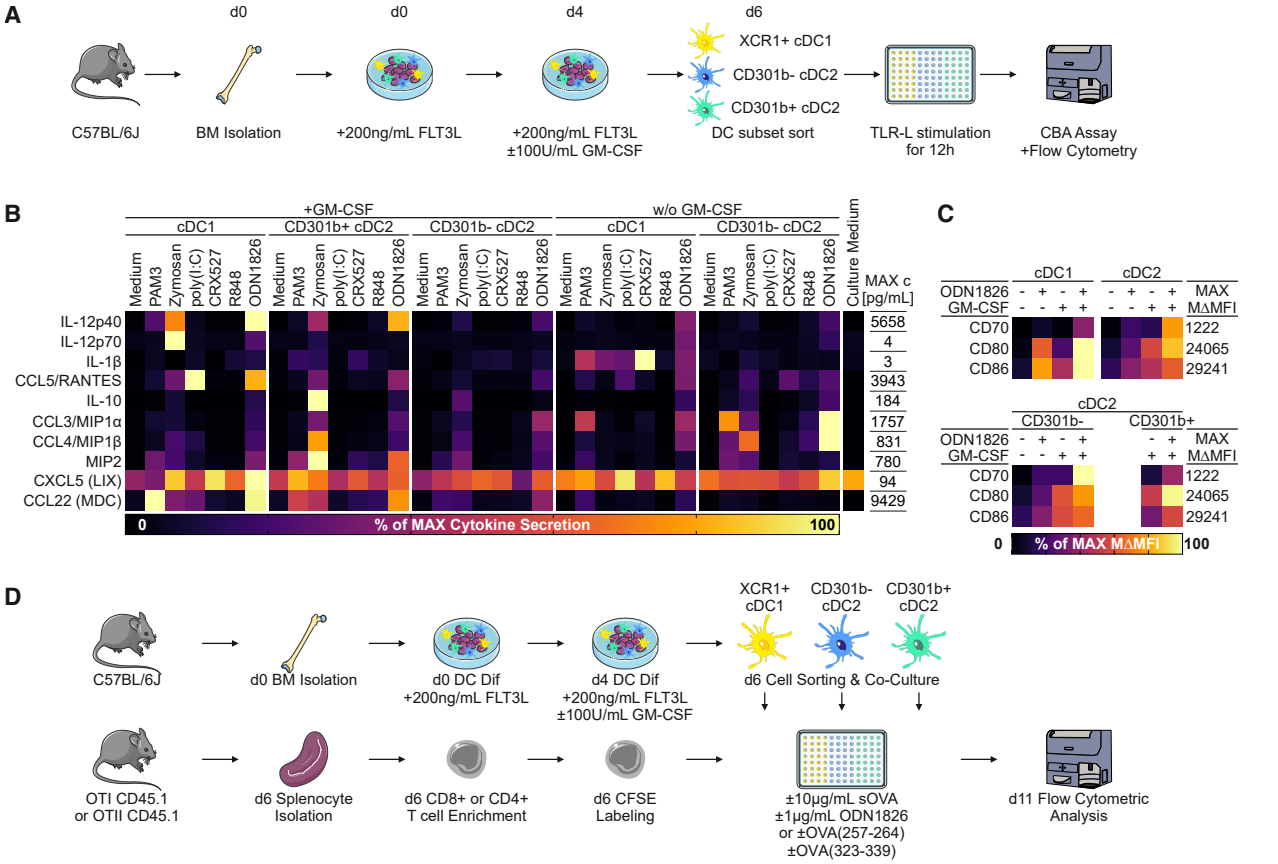
(E) Bubble plot visualizing homogeneity and protein expression strength on cDC subsets. The percentage of positive cells was extracted in comparison to mixed isotype controls/FMOs. Expression strength was determined by calculating ΔMFIs ($MFI_{staining} - MFI_{mixed\ isotype/FMO}$) followed by mean calculation of the biological replica. The highest resulting value (MΔMFI; displayed) on analyzed populations was set to 100% for normalization. $n_{differentiated\ cDC\ subsets} = 3$ biological replica; $n_{splenic\ cDCs\ for\ alignment} = 1$.

(F) PCA based on data in (E) utilizing expression strength (left) or expression pattern (right) as input.

(G) Output quantification (d6) of BM differentiation with FLT3L (d0), GM-CSF (d0), or FLT3L (d0) +GM-CSF (d4). BM was isolated from CD11c^{CRE}xIRF4$^{fl/fl}$ mice. n = 4–5 biological times 1–3 technical replicas. Unmatched, non-parametric Kruskal-Wallis test followed by Dunn's multiple comparisons test was used for statistical analysis. *$p \leq 0.05$; **$p \leq 0.01$; and ***$p \leq 0.001$. Medians ± interquartile range.

BM, bone marrow; FLT3L, FMS-like tyrosine kinase 3 ligand; GM-CSF, granulocyte/macrophage colony-stimulating factor; w/o, without; Norm., normalized; d, day; PC, principal component; PCA, principal component analysis; POS., positive; MAX, maximum; M., mean; SP, spleen; UMAP, uniform manifold approximation and projection; TF, transcription factor; R, receptor; TLR, Toll-like receptor; and CLR, C-type lectin receptor.

CellPress
OPEN ACCESS



(legend on next page)

via ODN1826, GM-CSF-differentiated cDC1s and cDC2s were superior in priming of $CD8^+$ T cells compared to their counterparts differentiated in the absence of GM-CSF. Additionally, we co-cultured sorted cDC subsets with $OVA_{323-339}$-specific $CD4^+$ T cells (Figures 2G and 2H). In general, GM-CSF-based differentiation strongly boosted the $CD4^+$ T cell priming ability of all cDC subsets in cultures relying on peptide pulsing or sOVA feeding.

In summary, GM-CSF modulated cytokine patterns produced by DCs in response to infection mimics and generally boosted their co-stimulatory capacity, equalizing the $CD8^+$ and $CD4^+$ T cell priming abilities of sorted cDC1 and cDC2 subsets upon soluble antigen uptake *ex vivo*.

Tissue $CD103^-$ cDC1s and $CD301b^-$ cDC2s are incapable of differentiating into $CD103^+$ cDC1 and $CD301b^+$ cDC2

We next questioned whether $CD103^+$ cDC1s and $CD301b^+$ cDC2s arise from $CD103^-$ cDC1s and $CD301b^-$ cDC2s populating murine tissues. Therefore, we analyzed the expression of the GM-CSF receptor alpha chain responsible for GM-CSF recognition (CSF2RA/CD116) on cDCs across tissues to determine if all cDCs can sense GM-CSF (Figures 3A, 3B, and S3).[64,65] We found that all cDCs homogeneously expressed CSF2RA. Hence, we sorted splenic $CD103^-$ cDC1s, $CD301b^-Clec12A^+$ cDC2s, and $CD301b^-ESAM^+$ cDC2s (Figure 3C). Exposure to GM-CSF *in vitro* for 2 days in analogy to bone marrow differentiation revealed that cDC1s failed to acquire CD103 expression in dependence on GM-CSF, while their $CD8\alpha^+$ phenotype was maintained (Figures 3D and 3E). Moreover, all $Clec12A^+$ and $ESAM^+$ cDC2s remained negative for CD301b (Figures 3D and 3E). These results either pointed toward a DC-intrinsic inability for GM-CSF-dependent differentiation or might be attributed to lacking unknown factors produced by bone marrow-located bystander cells in response to GM-CSF.

To investigate, if lacking bystander cells explain the inability of splenic cDCs to differentiate into $CD103^+$ cDC1s or $CD301b^+$ cDC2s, we cultured splenic $CD45.2^+$ cDCs either alone or on $CD45.1^+$ supplementing bone marrow or splenocytes in the presence or absence of FLT3L and GM-CSF (Figure 3F). In every case, $CD45.2^+$ cDCs were not developing in dependence on GM-CSF into $CD103^+$ or $CD301b^+$ cDCs (Figure 3G). However, we detected a significant increase in $CD45.1^+CD103^+$ and $CD45.1^+CD301b^+$ DCs within bone marrow bystander cells upon culturing with GM-CSF.

To understand, if the observed inability for GM-CSF-induced differentiation is an intrinsic feature of splenic cDCs, we differentiated $CD103^-$ cDC1s and $CD301b^-$ cDC2s from various tissues with FLT3L ± GM-CSF (Figures 3H, 3I, and S2B–S2E). As positive control, we cultured bone marrow since we showed that it responds to GM-CSF with CD103 and CD301b upregulation. While GM-CSF induced CD103 and CD301b expression in bone marrow, all sorted cDC1s and cDC2s remained negative for CD103 and CD301b post-differentiation independent of the tissue source. To exclude that viability issues explain the lack of *ex vivo* differentiation capacity, we analyzed cDC viability after passing our different differentiation systems by co-staining for 4′,6-diamidino-2-phenylindole (DAPI) and Annexin V. Apart from splenic bystanders, our results revealed that a considerable fraction of sorted cDCs was alive post-differentiation (~60%–80%) further increasing in the presence of GM-CSF (Figures S2F–S2I). Thus, we exclude that reduced viability accounts for the lack of differentiation in response to GM-CSF by cDCs *ex vivo*.

In summary, our results suggest a cDC-intrinsic inability to differentiate into $CD103^+$ cDC1s and $CD301b^+$ cDC2s upon GM-CSF stimulation, while developmentally earlier stages of cDCs might give rise to $CD103^+$ and $CD301b^+$ cDCs.

Pre-cDCs can transition into $CD103^+$ cDC1 and $CD301b^+$ cDC2

To address if earlier stages during cDC development differentiate into $CD301b^+$ cDC2s and $CD103^+$ cDC1s, we re-constructed a pre-cDC identification approach developed by Schlitzer et al. and applied it to analyze multiple murine tissues (Figures 4A, 4B, and S1D).[5] Overall, pre-cDCs were separated into $Ly6C^-Siglec\text{-}H^-$ pre-cDC1, $Ly6C^+Siglec\text{-}H^-$ pre-cDC2, $Ly6C^+Siglec\text{-}H^+$ pre-cDC1/2, and a $Ly6C^-Siglec\text{-}H^+$ population of pre-cDC/pDCs mainly consisting of contaminating CLP-derived pre-pDCs (Figures 4A, 4B, and S1D).[66] Apart from the lung, we could detect the different pre-cDC populations across murine tissues displaying a high frequency of pre-cDC1/2s in the bone marrow, while other tissues were mainly populated by later differentiation stages (Figures 4B and 4C). Thus, we focused on pre-cDC1s and pre-cDC2s and assessed when they express CSF2RA, CD103, or CD301b (Figure 4D). We found that pre-cDC1s and pre-cDC2s expressed CSF2RA across all tissues, while CD103 and CD301b were absent even after seeding peripheral tissues. In summary, $CSF2RA^+$ $CD103^-CD301b^-$ pre-cDCs populate murine tissues.

Figure 2. GM-CSF modulates DC cytokine production and equalizes the T cell priming capacity of cDC1s and cDC2s

(A) Workflow of cytokine measurements.

(B) Cytokine profile of cDC subsets displayed as percentage of maximum mean cytokine production in pg/mL. n = 5–6 biological replica.

(C) Co-stimulatory molecule expression displayed as percentage of maximum median ΔMFI (MΔMFI). n = 3 biological replica.

(D) Workflow of DC:T cell co-cultures.

(E–H) cDC subsets were either co-cultured with $OVA_{257-264}$-specific $CD8^+$ T cells (E) ±$OVA_{257-264}$ peptide or (F) sOVA and ODN1826 or with $OVA_{323-339}$-specific $CD4^+$ T cells (G) ±$OVA_{323-339}$ peptide or (H) sOVA and ODN1826. All co-cultures: n = 5 (DCs) or 2–3 (T cells) biological replica.

(F) $CD8^+$ T cell:DC ratio 8:1. (H) $CD4^+$ T cell:DC ratio 4:1.

(B) Mean.

(E and G) Median.

(F and H) Median ± 5th–95th percentile. A non-parametric Friedman test for paired samples followed by Dunn's post hoc test was performed within related groups (separated by dashed line). BM, bone marrow; Dif, differentiation; DC, dendritic cell; FLT3L, FMS-like tyrosine kinase 3 ligand; GM-CSF, granulocyte/macrophage colony-stimulating factor; d, day; sOVA, soluble OVA; and ODN1826, TLR9 ligand.

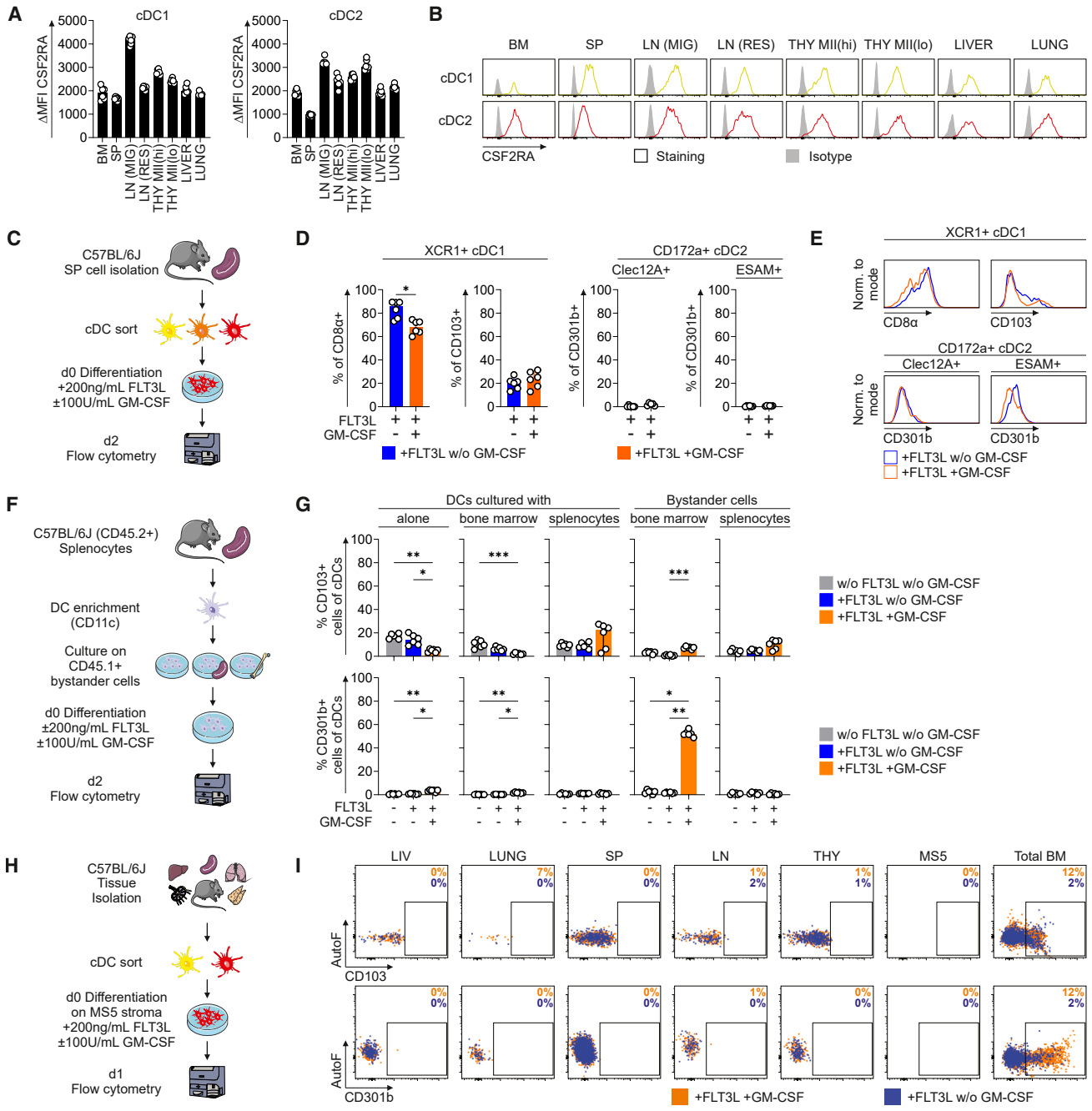


Figure 3. cDCs feature a cell-intrinsic inability to respond to GM-CSF by failing to differentiate into CD103$^+$ cDC1s or CD301b$^+$ cDC2s

(A and B) CSF2RA (CD116) on DCs from C57BL/6J mice. (A) Median ± interquartile range of 6 biological replicas.

(C) Workflow of splenic cDC subset differentiation.

(D) Percentage of CD103/CD8α/CD301b-positive DC subsets. *n* = 6 biological replica. Statistical significance was assessed using a two-tailed Wilcoxon test for paired samples. Medians ± interquartile range.

(E) Representative histograms of CD301b or CD103.

(F) Workflow of differentiation of splenic DCs on bystander cells.

(G) Percentage of CD103$^+$ and CD301b$^+$ cDCs in CD45.2$^+$CD11c$^+$ or CD45.1$^+$ bystander cells. *n* = 6 biological replicas. Non-parametric Friedman test for paired samples, followed by Dunn's post hoc test, was performed to assess statistical significance. Medians ± interquartile range.

(H) Workflow of tissue cDC differentiation.

(legend continued on next page)

Next, we tested if pre-cDC1s and pre-cDC2s develop into CD103$^+$ cDC1s and CD301b$^+$ cDC2s upon GM-CSF exposure (Figures 4E–4G and S1E–S1G). The data revealed that bone-marrow-isolated pre-cDC1s and pre-cDC2s gave rise to vast amounts of CD103$^+$ cDC1s and CD301b$^+$ cDC2s (Figure 4F). Further, GM-CSF slightly increased the frequency of CD103$^+$ cells within cDC1s and of CD301b$^+$ cells within cDC2s (Figure 4G). Thus, pre-cDC1s and pre-cDC2s are capable of upregulating CD103 and CD301b. Taken together, pre-cDC1s and pre-cDC2s represent direct progenitors of GM-CSF-dependent CD103$^+$ cDC1s and CD301b$^+$ cDC2s.

Pro-DC3s and pre-cDC2s can give rise to CD301b$^+$ DCs

Even though we showed that pre-cDC2s can give rise to CD301b$^+$ cDC2s in response to GM-CSF, this did not exclude that other DC populations contribute to the pool of CD301b$^+$ cDC2s. Previously, it was demonstrated that splenic XCR1$^-$CD172a$^+$ cDC2s consist of two developmentally distinct populations comprising FcγRIIB/III$^-$ and FcγRIIB/III$^+$ cells, termed DC2s and DC3s, respectively.[11,50,60] To determine if CD301b$^+$ cells are present within DC2s and DC3s across tissues, we separated XCR1$^-$CD172a$^+$ cDC2s based on their FcγRIIB/III expression. Since FcγRIIB/III separation was so far validated for the spleen but not peripheral tissues, we here named FcγRIIB/III$^-$ cells as putative DC2s and FcγRIIB/III$^+$ cells as putative DC3s. On these cells, we investigated the expression of CD301b (Figure 5A). Both FcγRIIB/III$^+$ and FcγRIIB/III$^-$ cells harbored CD301b$^+$ cells. Since FcγRIIB/III is only established as a DC3 marker for splenic DCs,[60] we analyzed if FcγRIIB/III$^-$ or FcγRIIB/III$^+$ DCs align to their splenic counterparts in a variety of tissues based on relative protein expression differences (Figures S4A and S4B). Correlation and principal component analysis of relative expression differences suggested that the majority of FcγRIIB/III$^+$ DCs across tissues might phenotypically correspond to splenic FcγRIIB/III$^+$ DC3s, while FcγRIIB/III$^-$ DCs aligned with splenic FcγRIIB/III$^-$ DC2s (Figures S4C and S4D).

Previously, FcγRIIB/III$^-$ DC2s were described to arise via CDPs and classical pre-cDC2s, while FcγRIIB/III$^+$ DC3s developed via pro-DC3s from a Ly6C$^+$ fraction of MDPs.[50,60] As Clec9A expression was described in CDPs, Clec9a^{CRE}xRosa26$^{LSL-TdTomato}$ mice (Figure S5) allow for tracing the cDC lineage starting from the CDP stage.[6,67] To potentially distinguish between DC2 and DC3 progenitors and their progeny across tissues, we therefore analyzed bone marrow progenitors defined according to Liu et al. (2019)[4] and bone marrow and splenic DC progenitors and their progeny identified according to Liu et al. (2023)[60] in Clec9a$^{CREwt/tg}$xRosa26$^{LSL-TdTomatowt/tg}$ mice (Figures S5A, S6A, and S6D). As expected, we observed labeling of CDPs and pre-cDCs, while other progenitors like CLPs, CMPs, GMPs, GPs, cMoPs, and Ly6C$^-$ MDPs in bone marrow and various cell types in the periphery were tomato negative, confirming specificity (Figures S5B–S5D). Of note, Ly6C$^+$ MDPs and pro-DC3s also showed prominent tomato labeling, while cMoPs and Ly6C^{high} monocytes were not labeled (Figures S5C and S5D). Consequently, splenic pre-cDCs and cDCs as well as pro-DC3s and DC3s were TdTomato$^+$. Finally, we observed that potential FcγRIIB/III$^-$ DC2s and FcγRIIB/III$^+$ DC3s (as defined in Figure S3) showed a high labeling throughout tissues, consistent with the TdTomato labeling of their progenitors in the bone marrow (Figures S5E and S5F). Hence, the Clec9a^{CRE}-based fate mapping approach strongly labels DC2s, DC3s, and their progenitors implying that DC3s are part of the Clec9a-traced DC pool that is distinct from monocytes. Collectively, our results suggest that CD301b$^+$ cells are found within FcγRIIB/III$^-$ (putative DC2s) and FcγRIIB/III$^+$ (putative DC3s) DCs in various tissues.

To identify the developmental stage at which CD301b$^+$ cells differentiate within the DC3s, we mapped DC3 progenitors within bone marrow as described previously.[60,68] Initially, Menezes et al. identified three monocyte populations termed R1, R2, and R3 monocytes giving rise to inflammatory macrophages, monocyte-derived DCs, or bona fide cDC2s, respectively.[68] Later, Liu et al. unraveled that R3 monocytes overlap with classical pre-cDC2s, whereas R2 monocytes equal pro-DC3s.[60] After validating in our own gating that pro-DC3s and pre-cDC2s equal R2 and R3 monocytes, we investigated if and at which stage CSF2RA and CD301b are expressed within the DC3 lineage (Figures 5B, S6A, and S6B). Our data showed that CSF2RA expression started within Ly6C$^+$ MDPs and was maintained afterward. However, CD301b was absent on all DC2 and DC3 progenitors but present on DC3s across tissues (Figures 5B–5D, S6C, and S6D).

To provide evidence that CD301b$^+$ cells develop from DC3 progenitors, we differentiated pro-DC3s and pre-cDC2s from bone marrow and spleen *ex vivo* (Figures 5E–5G and S6E–S6I). As for sorting of pre-cDC1s and pre-cDC2s, culture with MS5 stroma cells alone was sufficient to induce CD301b$^+$ expression on developing cells, suggesting that MS5 cells represent a useful tool to actively enforce CD301b$^+$ DC differentiation in the absence of external GM-CSF (Figures S6H and S6I). Most importantly, GM-CSF drove the expression of CD301b on cells developing from pro-DC3s and pre-cDC2s in both MS5 and CD45.1$^+$ bystander bone-marrow-based differentiation systems (Figures 5F, 5G, and S6H). In summary, our results suggest that CD301b$^+$ DCs develop from pre-committed DC3 and DC2 progenitors *ex vivo*.

GM-CSF sensing is selectively required by lung DCs to drive CD103 and CD301b expression

After demonstrating that GM-CSF, but not IRF4, is essential for the generation of CD301b$^+$ cDC2s and CD103$^+$ cDC1s *in vitro*, we addressed their importance under physiological conditions. Since the identification of putative DC2s and DC3s via FcγRIIB/III expression required further validation, we went

(I) CD103 on cDC1s (top) and CD301b on cDC2s (bottom) post-differentiation. Data representative for 3 biological replicas. Positive control: total bone marrow. FLT3L, FLT3-ligand; GM-CSF, granulocyte/macrophage colony-stimulating factor; cDC, conventional dendritic cell; SP, spleen; BM, bone marrow; THY, thymus; LN, lymph node; MIG, migratory; RES, resident; MII(hi), MHCII(high); MII(lo), MHCII(low); w/o, without; d, day; Norm., normalized; and AutoF, autofluorescence channel. *$p \leq 0.05$; **$p \leq 0.01$; and ***$p \leq 0.001$.

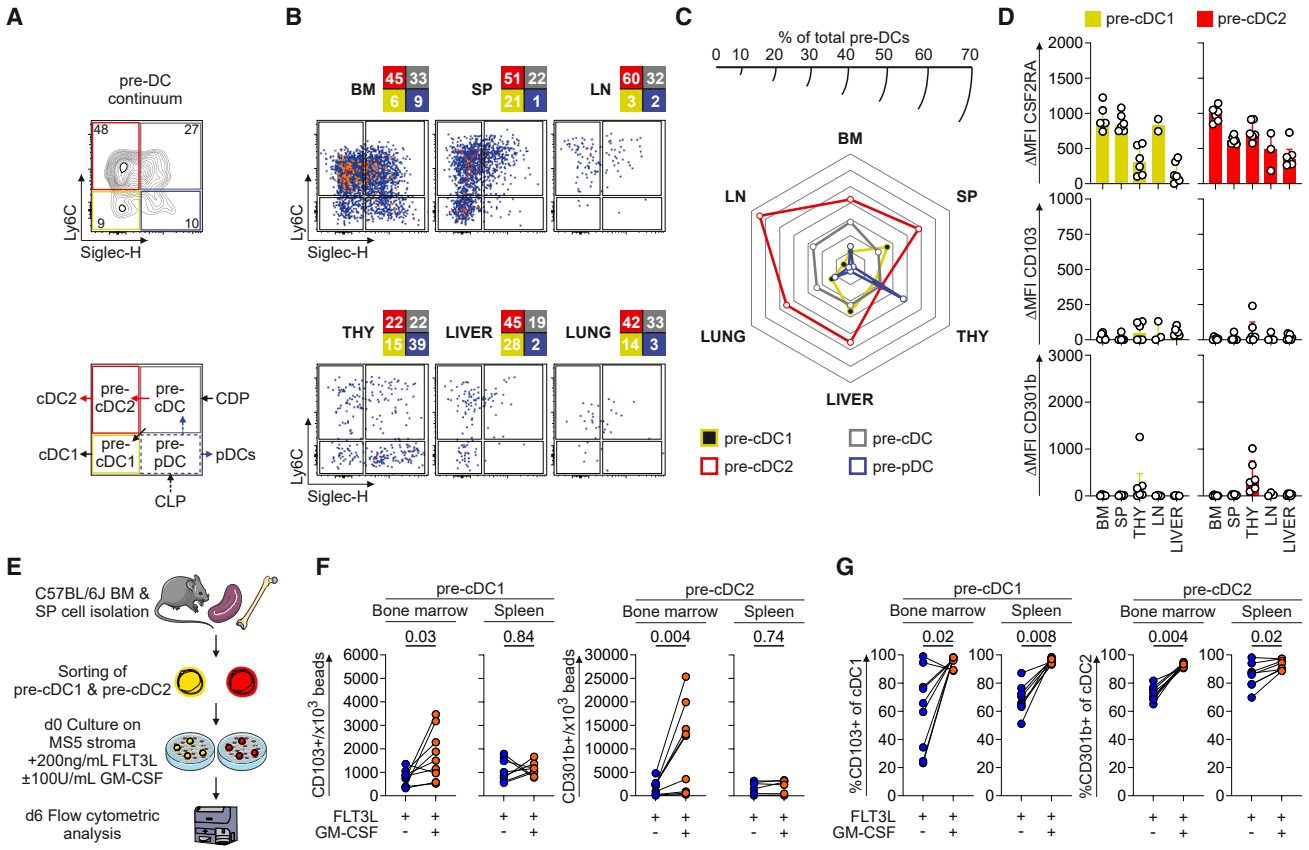


Figure 4. GM-CSF-sensitive pre-cDCs acquire CD103 or CD301b expression during their transition into DC1s and DC2s

(A) Schematic pre-cDC space. Ly6C$^-$Siglec-H$^-$, pre-cDC1s; Ly6C$^+$Siglec-H$^-$, pre-cDC2s; Ly6C$^+$Siglec-H$^+$, pre-cDCs; and Ly6C$^-$Siglec-H$^+$, pre-pDCs.

(B and C) Pre-cDC distribution visualized as (B) representative scatter dot plot or (C) spider chart displaying the mean frequency of pre-DC subsets within total pre-DCs per tissue. *n* = either 6 (BM/SP/THY/LIV) or 3 (lung/LNs) biological replicates each with 2 technical replicas.

(D) Expression (ΔMFI) of CSF2RA, CD103, and CD301b on pre-cDCs. Medians ± interquartile range. *n* = 2–3 (LNs) and 5–6 (other tissues) biological replicas.

(E) Workflow of pre-cDC differentiation.

(F and G) Quantitative (F) and qualitative (G) output quantification of CD103$^+$ cDC1s and CD301b$^+$ cDC2s. Measured cell counts of CD103$^+$ cDC1 and CD301b$^+$ cDC2 were normalized to a fixed amount of precision count beads. *n* = 8 (SP) or 9 (BM) biological replicas. Statistical significance was assessed utilizing two-tailed Wilcoxon test for paired non-parametric data.

cDC, conventional dendritic cells; pDC, plasmacytoid dendritic cells; BM, bone marrow; SP, spleen; THY, thymus; LN, skin-draining lymph nodes; FLT3L, Fms-related tyrosine kinase 3 ligand; GM-CSF, granulocyte/macrophage colony-stimulating factor; and d, day.

back to study CD301b$^+$ cells as a function of XCR1$^-$CD172a$^+$ cDC2s potentially comprising both DC2s and DC3s. By analyzing CD11c$^{CREwt/tg}$xIRF4$^{fl/fl}$ mice, we found that loss of IRF4 in CD11c-expressing cells did not block the differentiation of CD301b$^+$ cDC2s, even though their contribution to tissue cDC2 pools was reduced (Figures S7A and S7B). Moreover, we assessed the importance of GM-CSF in CD301b$^+$ cDC2 and CD103$^+$ cDC1 differentiation by studying tissue DCs in GM-CSF-deficient mice (Figures S7C–S7H). GM-CSF deficiency reduced the proportion of CD103$^+$ cells to total cDC1 pools and the expression of CD103 on cDC1s in a variety of tissues (Figures S7C, S7D, and S7G). While CD301b expression was modestly decreased in a variety of tissues, we only registered a reduction in the proportion of CD301b$^+$ cells within lung cDC2s (Figures S7E, S7F, and S7H). To understand if the importance of GM-CSF for CD103$^+$ cDC1 and CD301b$^+$ cDC2 differentiation is DC intrinsic, we made use of newly generated CD11c$^{CREwt/tg}$xCSF2Rα$^{fl/fl}$ mice in which the GM-CSF receptor alpha chain is conditionally deleted within CD11c-expressing cells. Thereby, CSF2Rα depletion is mostly limited to DCs, while cells remain signaling competent post IL3 and IL5 recognition. Thus, CD11c^{CRE}xCSF2Rα$^{fl/fl}$ mice represent a clear advantage over classical GM-CSF biology models (CSF2$^{-/-}$, CSF2Rα$^{-/-}$, and CSF2Rβ$^{-/-}$ mice). Tissue DC analysis revealed that DC-intrinsic GM-CSF sensing was essential for lung cDCs, as marked by strong reductions of CD103 and CD301b expression and the contribution of CD103$^+$ and CD301b$^+$ cells to cDC1s and cDC2s, respectively (Figures 6A–6D).

Overall, lung cDCs harbored a DC-intrinsic requirement for GM-CSF sensing, while yet-unknown factors compensate for a loss of GM-CSF sensing by DCs in other tissues. Additionally, these results suggested the existence of an alternative mechanism allowing for the generation of CD301b$^+$ cDC2s, but not CD103$^+$ cDC1s.

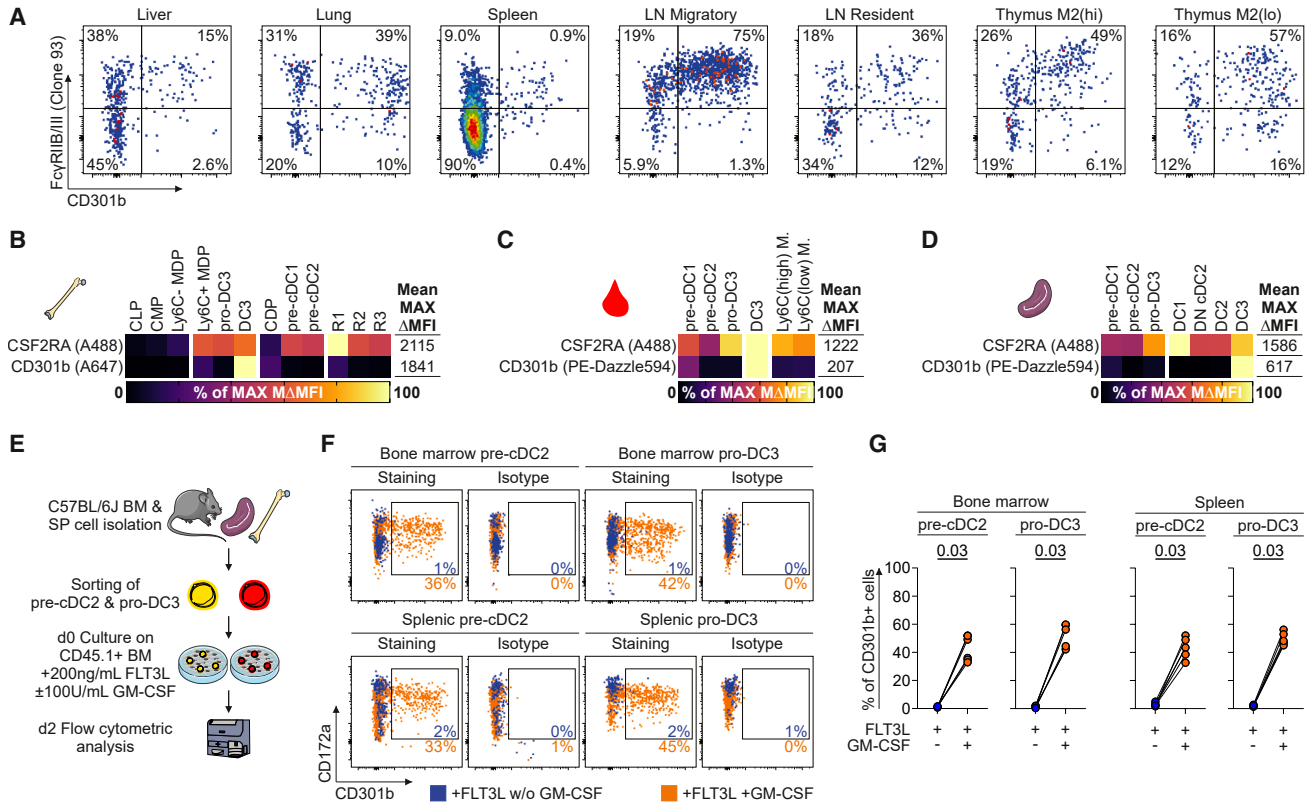


Figure 5. CD301b$^+$ cells develop from DC2- and DC3-committed progenitors

(A) CD301b vs. FcγRIIB/III on XCR1$^-$CD172a$^+$ DCs. Representative for 6 biological replicas.

(B–D) Expression of CSF2RA and CD301b on cells within (B) bone marrow, (C) blood, and (D) spleen. *n* = 5 (B), 3 (C), and 6 (D) biological replicas. All expression data are displayed as percentage of maximum mean ΔMFI on the listed cell populations.

(E) Workflow of DC progenitor differentiation.

(F) Representative dot plot visualizing CD301b expression on differentiated cells.

(G) Percentage of CD301b$^+$ cells post *ex vivo* differentiation. *n* = 6 biological replicas. Paired, two-tailed Wilcoxon matched-pairs signed-rank test was used to test for statistical significance.

cDC, conventional dendritic cells; pDC, plasmacytoid dendritic cells; CDP, common dendritic cell precursor; CLP, common lymphoid progenitor; CMP, common lymphoid progenitor; MDP, monocyte-dendritic cell progenitor; M., monocytes; MAC, macrophage; % of MAX MΔMFI, percentage of the maximum mean delta mean fluorescence intensity; BM, bone marrow; SP, spleen; LIV, liver; LN, skin-draining lymph nodes; THY, thymus; R1 monocyte, monocyte-lineage progenitor; R2 monocyte, pro-DC3s; R3 monocyte, pre-cDC2s; and w/o, without.

Specific type 2 cytokines can compensate for GM-CSF in inducing CD103 and CD301b expression

Thus, we investigated which factors compensate for the actions of GM-CSF in differentiating CD103$^+$ cDC1s and CD301b$^+$ cDC2s. Owing to their close linkage to GM-CSF biology, we picked IL3, IL4, IL5, and IL13 as candidates. While IL3 and IL5 signal via the same receptor common beta chain (CD131/CSF2Rβ) as GM-CSF, the genes for IL4 and IL13 cluster with GM-CSF on the same chromosome, where their expression is coordinately regulated.[69,70] We tested the ability of these cytokines to generate CD103$^+$ cDC1s and CD301b$^+$ cDC2s *in vitro* by cross-comparing them to GM-CSF during bone-marrow-based DC differentiation (Figures 7A–7D). We identified IL3 as a compensatory factor driving CD103 expression on cDC1s (Figures 7A–7D). Moreover, IL3, IL4, and IL13 generated CD301b$^+$ cDC2s (Figures 7A–7D). These observations were supported by the finding that, at the time point of cytokine supplementation, differentiating cDC1s were only equipped to recognize IL3, whereas cDC2s expressed the necessary receptor chains to sense IL3, IL4, and IL13 (Figures 7E and 7F).

In conclusion, our results suggest that lung CD103$^+$ cDC1s and CD301b$^+$ cDC2s have a cell-intrinsic requirement for GM-CSF sensing, while in other tissues, additional cytokines might compensate for the actions of GM-CSF in a DC-subset-specific manner.

DISCUSSION

Here, we delineated the timing, location, cellular origin, and regulatory factors governing the development of CD103$^+$ cDC1s and CD301b$^+$ cDC2s. By establishing an *in vitro* platform capable of generating all cDC subsets, including *bona fide* CD301b$^+$ cDC2s, we highlight GM-CSF as a driver of CD103$^+$

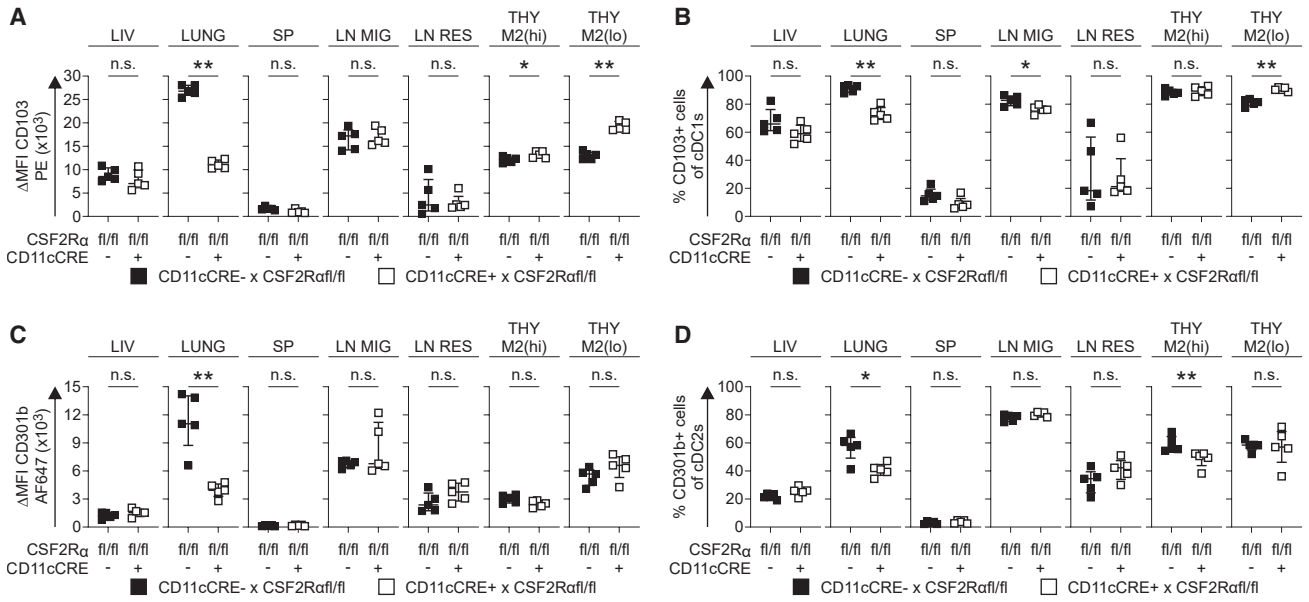


Figure 6. Lung DCs require DC-intrinsic GM-CSF sensing to acquire CD103 and CD301b expression

Flow cytometric analysis of cDCs in CD11c^{CRE}xCSF2Rα$^{fl/fl}$ mice. $n = 5$ biological replica per genotype. A non-parametric, unpaired, two-tailed Mann-Whitney test was used to compare ranks. *$p \leq 0.05$; **$p \leq 0.01$. Median ± interquartile range.

(A) ΔMFI of CD103 on cDC1s.

(B) Percentage of CD103$^+$ cells within cDC1s.

(C) ΔMFI of CD301b on cDC2s.

(D) Percentage of CD301b$^+$ cells within cDC2s.

LN, skin-draining lymph nodes; THY, thymus; LIV, liver; SP, spleen; MIG, migratory; RES, resident; M2(hi), MHCIIhigh; M2(lo), MHCIIlow; ΔMFI, delta mean fluorescence intensity; and n.s., not significant.

cDC1 and CD301b$^+$ cDC2 development. GM-CSF boosted the T cell priming capacity of these populations while remodeling their cytokine profiles. As CD301b$^+$ cells arise from pre-committed DC2 and DC3 progenitors upon GM-CSF encounter *ex vivo*, our data indicate that CD301b marks a GM-CSF-associated state within the ontogenetically distinct DC2 and DC3 lineages. Finally, we show that lung DCs require DC-intrinsic GM-CSF sensing to induce CD103 and CD301b expression, whereas cytokines such as IL3, IL4, and IL13 can compensate for the absence of GM-CSF signaling *ex vivo*.

A differentiation platform for bona fide cDCs *in vitro* enables the study of distinct DC repertoires

In vitro differentiation platforms have a long history in studying development and function of scarce DC populations.[34,61,62,71–73] Besides the essential DC growth factor FLT3L, previous studies showed that GM-CSF is associated with establishing and maintaining border tissue DC pools, including CD103$^+$ cDC1s and CD301b$^+$ cDC2s.[34,61,62,74–79] However, the value of GM-CSF-based culturing protocols was challenged by the finding that GM-CSF primarily facilitates monocyte-derived macrophage generation from monocyte progenitors outnumbering DC lineage progenitors in bone marrow.[63] Our bone marrow differentiation platform based on sequential provision of FLT3L followed by GM-CSF allows for overcoming this issue by generating bona fide cDC1s and cDC2s that are strictly dependent on FLT3L and display a high expression of classical DC markers (ZBTB46/CD26/DCIR1), whereas monocyte/macrophage-associated proteins (MerTK/MafB/CD88/Ly6C/VISTA) are absent.[9,11,51,54,63,80]

Moreover, GM-CSF facilitated the generation of CD103$^+$ cDC1s and CD301b$^+$ cDC2s. In the literature, high shares of CD103$^+$ cDC1s and CD301b$^+$ cDC2s were described within non-sterile barrier tissues.[11,13,34,35,74–76,79] Considering that sub-classification into cDC1s and cDC2s had the highest impact on their protein signature followed by GM-CSF presence, this indicates that GM-CSF, which is absent from the circulation during homeostasis but is present within barrier tissues, contributes to the phenotypic fine-tuning of DC subsets observed within select tissue environments.[11,65,81,82] In summary, our results reveal that *in vitro* differentiation systems employing FLT3L alone or in combination with delayed GM-CSF supply allow for the development and study of cDC repertoires usually identified within lymphoid or barrier tissues, respectively.

GM-CSF rewires and boosts cDC functionality

In mice, cDC1s are described as major inducers of CD8$^+$ T cell responses.[2,17,18,21,31,83] While the GM-CSF-dependent acquisition of CD103 was already previously associated with increased cross-presentation by cDC1s,[62,84] GM-CSF boosted the CD8$^+$ and CD4$^+$ T cell priming capacity of all analyzed cDC1 and cDC2 subsets to equal levels, potentially via increasing their co-stimulatory potential. Considering that the

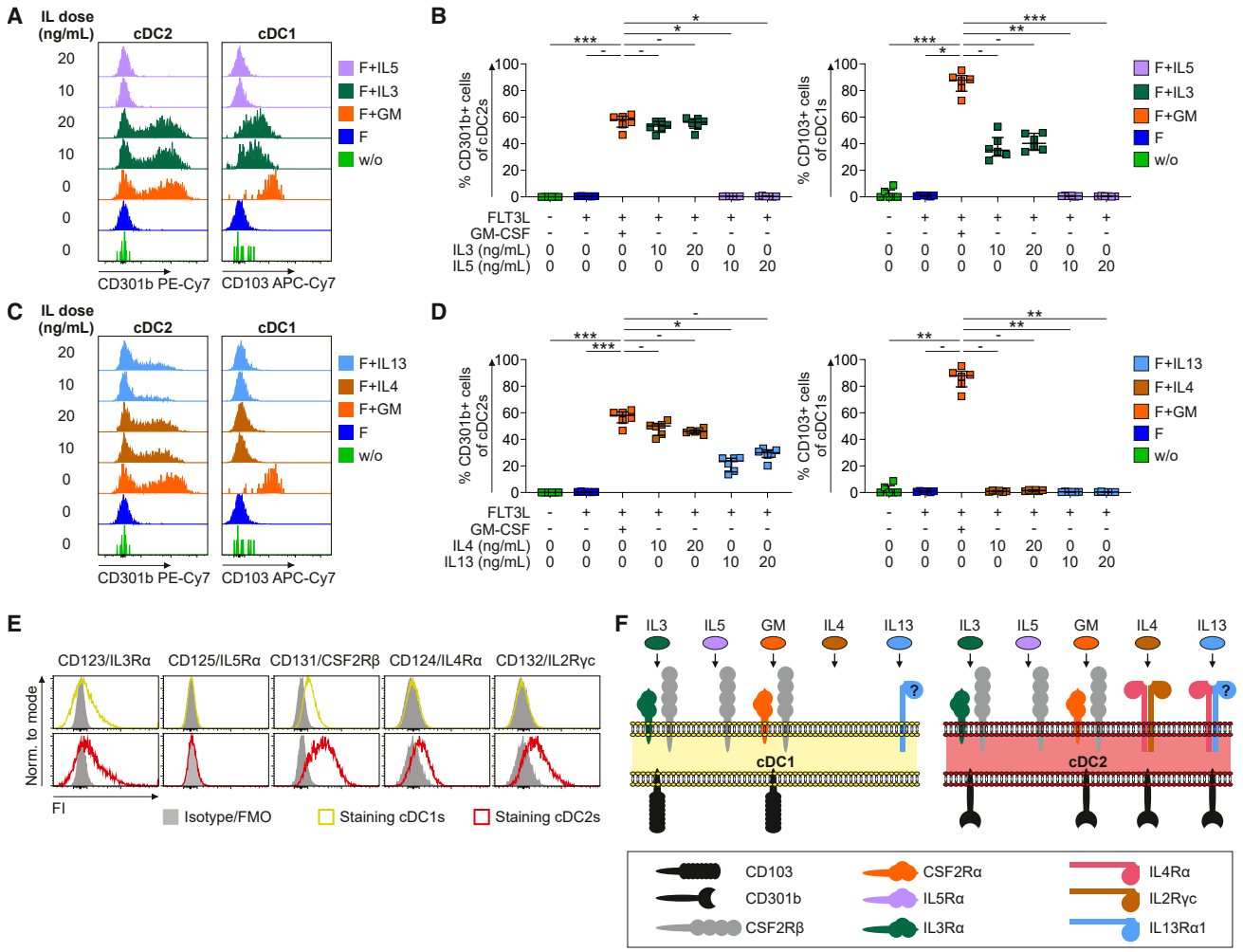


Figure 7. Specific type 2 cytokines drive CD103 and CD301b expression on cDC1s and cDC2s, respectively

(A–E) C57BL/6J bone marrow was differentiated with FLT3L before additional cytokines were added at day 4 followed by flow cytometry at day 6.

(A and C) Expression of CD301b on cDC2s and CD103 on cDC1s. Data are representative for 6 biological replicas.

(B and D) Percentage of CD301b$^+$ cells within cDC2s and of CD103$^+$ cells within cDC1s. $n = 6$ biological replicas. A matched, non-parametric Friedman test in combination with Dunn's multiple comparisons test was performed to cross-compare all conditions to FLT3L + GM-CSF. $^*p \leq 0.05$; $^{**}p \leq 0.01$; $^{***}p \leq 0.001$. Median ± interquartile range.

(E) Expression of cytokine receptor chains on cDC1s and cDC2s on day 4 of bone marrow differentiation with FLT3L.

(F) Model summarizing cytokine receptor and downstream expression of CD103 on cDC1s and CD301b on cDC2s.

w/o, without; F, FLT3L; GM, GM-CSF; IL, interleukin; FI, fluorescence intensity; Norm., normalized; and FMO, fluorescence minus one.

GM-CSF-dependent phenotypes of DCs are predominantly found in barrier tissues,[65] while they in parallel display a boosted capacity to prime T cells, CD103$^+$ cDC1s and CD301b$^+$ cDC2s might represent highly specialized guardians of mucosal tissues. Overall, CD301b$^+$ cDC2s have been described to operate at both ends of the immunological spectrum by driving T_H2 and T_H17 responses and by contributing to peripheral and central tolerance.[33–35,85–87] The expression of CD301b itself enables the recognition of N-acetylgalactosamine, an amino sugar frequently present on self-antigens endowing DCs with the capability to recognize certain tumor-associated glycans.[88–90] Thus, the question arises whether CD301b$^+$ cDC2s are pro- or anti-tumorigenic.

Pre-cDC2s and pro-DC3s give rise to CD301b$^+$ DCs upon GM-CSF exposure *ex vivo*

To clarify, whether CD301b tags an ontogenetically distinct cDC2 population or refers to a GM-CSF-associated state, we set out to determine the time point, location, and cell population giving rise to CD301b$^+$ cDC2s. We identified pre-cDC2s as their direct progenitors. This is in accordance with a previous study demonstrating that differentiation of bone marrow pre-cDCs in the presence of FLT3L and GM-CSF *in vitro* facilitated the generation of CD301b$^+$ cDC2s.[34] *In vivo*, CD301b$^+$ cDC2s are found at varying frequencies in different tissues.[11,34,35,39] Considering that pre-cDC2s, which seed peripheral tissues following their bone marrow egress,[5,60] were homogenously GM-CSF sensitive

(CSF2RA$^+$) but negative for CD301b, these results imply that pre-cDC2s differentiate into CD301b$^+$ cDC2s after encountering local GM-CSF within their target tissue. Additionally, adoptive transfer settings have previously shown that CD301b$^+$ DCs can arise from Ly6C$^+$ cells potentially representing pre-cDC2s, while CD301b$^+$ DCs could develop into CD301b$^-$ cells. Together with our findings presented here, these results suggest that CD301b$^-$ cDC2s are incapable of re-expressing or initiating expression of CD301b.[91] Importantly, we could generate CD301b$^+$ cells from pro-DC3s *ex vivo* in response to GM-CSF rendering CD301b$^+$ cells as a cytokine-induced cell state that does not represent a distinct lineage of DCs, additionally implying that CD301b$^+$ DC3 development occurs between the pro-DC3 and DC3 stage. Finally, fate-mapping data in Clec9a^{CRE}xRosa26$^{LSL-TdTomato}$ mice displayed prominent labeling of DC3 progenitors in bone marrow (Ly6C$^+$ MDPs, pro-DC3s) and of putative DC3s in lymphoid and non-lymphoid tissues, whereas monocyte progenitors and their progeny were not labeled. Even though Clec9a-based fate mapping does thus not allow for segregating DC2s and DC3s, these data demonstrate that Ly6C$^+$ MDPs, pro-DC3s, and DC3s are part of the Clec9a-traced DC compartment that is distinct from monocytes.

T_H2-associated cytokines can drive CD301b$^+$ cDC2 differentiation in the absence of DC-intrinsic GM-CSF recognition in a tissue-dependent manner

By using novel CD11c^{CRE}xCSF2R$\alpha^{fl/fl}$ mice, we demonstrated that only lung cDC2s required DC-intrinsic GM-CSF sensing to drive CD301b expression, implying the existence of compensatory mechanisms in other tissues. We found that IL3, which is signaling via the same receptor β-chain as GM-CSF, as well as IL4 and IL13, which are located on the same chromosome as GM-CSF, where their expression is coordinately regulated, can induce CD301b expression on FLT3L-differentiated DCs.[69,70] Previous studies already described cDC2 subsets requiring classical type 2 cytokine signals. These include CD11b^{low} dermal cDC2s that, in contrast to cDC2s from the lung and intestine, required IL13 and thymic CD301b$^+$ cDC2s relying on IL4 receptor signaling during homeostasis.[85,92] Overall, this raises the question if CD301b$^+$ cDC2s represent a conserved functional state across tissues or harbor tissue-specific requirements for GM-CSF, IL3, IL4, and IL13. Moreover, considering that GM-CSF and IL3 mainly act via Janus kinase (JAK) 2 and downstream signal transducers and activators of transcription (STAT) 5, while IL4 or IL13 act either via JAK1/JAK3 or JAK1/JAK2 mainly on STAT6, the question arises if these cytokines drive individual transcriptional signatures within DCs.[93–97] Finally, differences in the underlying signatures might translate to altered functional capacities potentially explaining tissue- and model-specific roles of CD301b$^+$ cDC2s in tolerance induction or the initiation of T_H2 and T_H17 responses.[34,35,85–87,98]

In summary, we established an *in vitro* platform generating bona fide CD103$^+$ cDC1s and CD301b$^+$ cDC2s, enabling analysis of their developmental trajectories and functional properties. We demonstrate that CD301b marks a cytokine-induced DC state arising during the transition from pre-cDC2s and pro-DC3s into DCs. Importantly, lung DCs uniquely require cell-intrinsic GM-CSF sensing for CD301b and CD103 expression, whereas IL3, IL4, and IL13 may compensate to induce CD301b expression. These results provide new insight into the cytokine-dependent regulation of functional dendritic cell states across tissues.

Limitations of the study

The description of putative DC2s and DC3s in our study is based on FcγRIIB/III expression and phenotypic alignment. Even though our results indicate that the majority of FcγRIIB/III$^+$ and FcγRIIB/III$^-$ DCs align with their splenic counterparts, lineage tracing (e.g., mapping of CD7 expression history), phenotypic cross-comparisons of tissue DC subsets to splenic reference DC2s and DC3s via scRNA sequencing, and DC-subset committed progenitor transfer experiments are required to reliably map DC2s and DC3s in a variety of tissues in the future.

RESOURCE AVAILABILITY

Lead contact

Further information and requests for resources and reagents should be addressed to and will be fulfilled by the lead contact, Diana Dudziak (diana.dudziak@med.uni-jena.de).

Materials availability

This study did not generate new, unique reagents.

Data and code availability

Data reported in this paper will be shared by the lead contact upon request. This paper does not report original code. Any additional information required to reanalyze the data reported in this paper is available from the lead contact upon request.

ACKNOWLEDGMENTS

Parts of this manuscript are part of the PhD thesis of Lukas Amon. We are thankful for the support of Markus Mroz and Uwe Appelt from the Core Unit Cell Sorting and Immunomonitoring of the Friedrich-Alexander-Universität Erlangen-Nürnberg and of Katrin Hornung from the Core Facility Cytometry of the Institute of Immunology at Jena University Hospital. We further thank several former members of the Dudziak laboratory for their general support, including Christina Gmeiner, Simone Dörfler, Katharina Hofmann, and Nathalie Eissing. We thank the Transgenic Core Facility at the VIB-UGent Center for Inflammation Research and in particular Tino Hochepied and Frédérique Van Rockeghem for the generation of the B6J-Csf2ra^{em1IRC} mouse line. Further, we thank the VIB Flow Core Ghent for their support. Cytokines employed from ImmunoTools were part of the ImmunoTools IT-Box-Cy55M awarded to Dr. Christian Lehmann by ImmunoTools. Schematic images utilized in figures are provided and adapted from Servier Medical Art (smart.servier.com), and these images are licensed under the Creative Commons Attribution 4.0 Unported License (creativecommons.org/licenses/by/4.0/). This study was funded by several grants, including Deutsche Forschungsgemeinschaft (German Research Foundation; DFG) and Agence Nationale de la Recherche (ANR) grant DU548/6-1 (431402787), DFG program TRR305 project B05 (429280966), DFG program TRR374 project B7 (509149993), DU548/9-1 (515982377), a fund from the Bavarian State Ministry of Science and Art Bayresq.Net "Project IRIS" to D.D., and DFG program RTG2504 (401821119) to D.D. and C.H.K.L. Further, D.D. is funded by the DFG under Germanyś Excellence Strategy – EXC 2051 – Project-ID 390713860. B.U.S. was supported by DFG program TRR 359 project B05 (491676693) and FOR2599 project P03 (SCHR 1444/2-1). B.N.L. was supported by European Research Council (ERC) advanced grant ERC-2017-ADG-789384, Excellence Science (EOS) research grants G0G2318N and GoH1222N, iBOF-FWO grant, and BOF Methusalem grant 01GA2817 - BOF17/GOOA/028. K.H. was supported by DFG - Projektnummer 505539112 (B03) and - Projektnummer 324392634 - TRR 221(B03) and TRR417-Project ID: 540805631-TP15.

AUTHOR CONTRIBUTIONS

Conceptualization, L.A., C.H.K.L., L.H., and D.D.; methodology, L.A., D.V., C.H.K.L., M.M., B.N.L., and D.D.; formal analysis, L.A.; investigation, L.A., D.V., A.S., G.T., M.M., L.L., L.H., N.D., N.K., T.V., K.R.R., and C.H.K.L.; resources, C.H.K.L., F.N., B.N.L., K.H., K.P., B.U.S., and D.D.; writing – original draft, L.A. and D.D.; writing – review & editing, L.A., D.V., A.S., L.H., G.T., T.K., S.E.A., M.M., N.D., N.K., T.V., N.R.T., F.N., K.R.R., K.H., K.P., B.U.S., B.N.L., C.H.K.L., and D.D.; visualization, L.A.; supervision, D.D.; and funding acquisition, C.H.K.L., B.U.S., K.H., B.N.L., and D.D.

DECLARATION OF INTERESTS

The authors declare no competing interests.

DECLARATION OF GENERATIVE AI AND AI-ASSISTED TECHNOLOGIES IN THE WRITING PROCESS

During revision, the authors used ChatGPT (GPT-4o-mini, OpenAI, 2025) solely to enhance language conciseness in newly added manuscript sections. After tool usage, all authors reviewed and edited the content. The authors take full responsibility for the content of the published article.

STAR★METHODS

Detailed methods are provided in the online version of this paper and include the following:

- KEY RESOURCES TABLE
- EXPERIMENTAL MODEL AND STUDY PARTICIPANT DETAILS
  - Mice
  - Generation of B6J-Csf2ra^{em1IRC} mice
  - Cell lines and cell culture
- METHOD DETAILS
  - Perfusion and tissue collection
  - Preparation of single-cell suspensions
  - Flow cytometry
  - Generation of cDCs from total bone marrow
  - Cell enrichment procedures and sorting
  - Differentiation assays of cDCs on supporting bone marrow and splenocytes
  - Differentiation assays of sorted pre-cDCs and pro-DC3s on bystander cells
  - T cell:DC co-culture assays
  - DC stimulation and cytokine measurements via CBA
- QUANTIFICATION AND STATISTICAL ANALYSIS

SUPPLEMENTAL INFORMATION

Supplemental information can be found online at https://doi.org/10.1016/j.celrep.2025.116589.

Received: February 10, 2025
Revised: September 2, 2025
Accepted: October 31, 2025
Published: November 26, 2025

REFERENCES

1. Guilliams, M., Ginhoux, F., Jakubzick, C., Naik, S.H., Onai, N., Schraml, B.U., Segura, E., Tussiwand, R., and Yona, S. (2014). Dendritic cells, monocytes and macrophages: a unified nomenclature based on ontogeny. Nat. Rev. Immunol. *14*, 571–578. https://doi.org/10.1038/nri3712.
2. Amon, L., Lehmann, C.H.K., Baranska, A., Schoen, J., Heger, L., and Dudziak, D. (2019). Transcriptional control of dendritic cell development and functions. Int. Rev. Cell Mol. Biol. *349*, 55–151. https://doi.org/10.1016/bs.ircmb.2019.10.001.
3. Anderson, D.A., 3rd, Dutertre, C.A., Ginhoux, F., and Murphy, K.M. (2021). Genetic models of human and mouse dendritic cell development and function. Nat. Rev. Immunol. *21*, 101–115. https://doi.org/10.1038/s41577-020-00413-x.
4. Liu, Z., Gu, Y., Chakarov, S., Bleriot, C., Kwok, I., Chen, X., Shin, A., Huang, W., Dress, R.J., Dutertre, C.A., et al. (2019). Fate Mapping via Ms4a3-Expression History Traces Monocyte-Derived Cells. Cell *178*, 1509–1525.e19. https://doi.org/10.1016/j.cell.2019.08.009.
5. Schlitzer, A., Sivakamasundari, V., Chen, J., Sumatoh, H.R.B., Schreuder, J., Lum, J., Malleret, B., Zhang, S., Larbi, A., Zolezzi, F., et al. (2015). Identification of cDC1- and cDC2-committed DC progenitors reveals early lineage priming at the common DC progenitor stage in the bone marrow. Nat. Immunol. *16*, 718–728. https://doi.org/10.1038/ni.3200.
6. Schraml, B.U., van Blijswijk, J., Zelenay, S., Whitney, P.G., Filby, A., Acton, S.E., Rogers, N.C., Moncaut, N., Carvajal, J.J., and Reis e Sousa, C. (2013). Genetic tracing via DNGR-1 expression history defines dendritic cells as a hematopoietic lineage. Cell *154*, 843–858. https://doi.org/10.1016/j.cell.2013.07.014.
7. Karsunky, H., Merad, M., Cozzio, A., Weissman, I.L., and Manz, M.G. (2003). Flt3 ligand regulates dendritic cell development from Flt3+ lymphoid and myeloid-committed progenitors to Flt3+ dendritic cells in vivo. J. Exp. Med. *198*, 305–313. https://doi.org/10.1084/jem.20030323.
8. Momenilandi, M., Levy, R., Sobrino, S., Li, J., Lagresle-Peyrou, C., Esmaeilzadeh, H., Fayand, A., Le Floc'h, C., Guerin, A., Della Mina, E., et al. (2024). FLT3L governs the development of partially overlapping hematopoietic lineages in humans and mice. Cell *187*, 2817–2837.e2831. https://doi.org/10.1016/j.cell.2024.04.009.
9. Guilliams, M., Dutertre, C.A., Scott, C.L., McGovern, N., Sichien, D., Chakarov, S., Van Gassen, S., Chen, J., Poidinger, M., De Prijck, S., et al. (2016). Unsupervised High-Dimensional Analysis Aligns Dendritic Cells across Tissues and Species. Immunity *45*, 669–684. https://doi.org/10.1016/j.immuni.2016.08.015.
10. Amon, L., Hatscher, L., Heger, L., Dudziak, D., and Lehmann, C.H.K. (2020). Harnessing the Complete Repertoire of Conventional Dendritic Cell Functions for Cancer Immunotherapy. Pharmaceutics *12*, 663. https://doi.org/10.3390/pharmaceutics12070663.
11. Amon, L., Seichter, A., Vurnek, D., Heger, L., Lächele, L., Tochoedo, N.R., Kaszubowski, T., Hatscher, L., Baranska, A., Tchitashvili, G., et al. (2024). Clec12A, CD301b, and FcgammaRIIB/III define the heterogeneity of murine DC2s and DC3s. Cell Rep. *43*, 113949. https://doi.org/10.1016/j.celrep.2024.113949.
12. Amon, L., Seichter, A., Vurnek, D., Tchitashvili, G., Heß, I., Heger, L., Lehmann, C.H.K., and Dudziak, D. (2024). Protocol for mapping the heterogeneous dendritic cell network across the murine tissue landscape via high-dimensional flow cytometry. STAR Protoc. *5*, 103151. https://doi.org/10.1016/j.xpro.2024.103151.
13. Edelson, B.T., Kc, W., Juang, R., Kohyama, M., Benoit, L.A., Klekotka, P.A., Moon, C., Albring, J.C., Ise, W., Michael, D.G., et al. (2010). Peripheral CD103+ dendritic cells form a unified subset developmentally related to CD8alpha+ conventional dendritic cells. J. Exp. Med. *207*, 823–836. https://doi.org/10.1084/jem.20091627.
14. Miller, J.C., Brown, B.D., Shay, T., Gautier, E.L., Jojic, V., Cohain, A., Pandey, G., Leboeuf, M., Elpek, K.G., Helft, J., et al. (2012). Deciphering the transcriptional network of the dendritic cell lineage. Nat. Immunol. *13*, 888–899. https://doi.org/10.1038/ni.2370.
15. Soares, H., Waechter, H., Glaichenhaus, N., Mougneau, E., Yagita, H., Mizenina, O., Dudziak, D., Nussenzweig, M.C., and Steinman, R.M. (2007). A subset of dendritic cells induces CD4+ T cells to produce IFN-gamma by an IL-12-independent but CD70-dependent mechanism in vivo. J. Exp. Med. *204*, 1095–1106. https://doi.org/10.1084/jem.20070176.

16. Lehmann, C.H.K., Heger, L., Heidkamp, G.F., Baranska, A., Lühr, J.J., Hoffmann, A., and Dudziak, D. (2016). Direct Delivery of Antigens to Dendritic Cells via Antibodies Specific for Endocytic Receptors as a Promising Strategy for Future Therapies. Vaccines (Basel) *4*, 8. https://doi.org/10.3390/vaccines4020008.

17. den Haan, J.M., Lehar, S.M., and Bevan, M.J. (2000). CD8(+) but not CD8(-) dendritic cells cross-prime cytotoxic T cells in vivo. J. Exp. Med. *192*, 1685–1696. https://doi.org/10.1084/jem.192.12.1685.

18. Dudziak, D., Kamphorst, A.O., Heidkamp, G.F., Buchholz, V.R., Trumpfheller, C., Yamazaki, S., Cheong, C., Liu, K., Lee, H.W., Park, C.G., et al. (2007). Differential antigen processing by dendritic cell subsets in vivo. Science *315*, 107–111. https://doi.org/10.1126/science.1136080.

19. Everts, B., Tussiwand, R., Dreesen, L., Fairfax, K.C., Huang, S.C.C., Smith, A.M., O'Neill, C.M., Lam, W.Y., Edelson, B.T., Urban, J.F., Jr., et al. (2016). Migratory CD103+ dendritic cells suppress helminth-driven type 2 immunity through constitutive expression of IL-12. J. Exp. Med. *213*, 35–51. https://doi.org/10.1084/jem.20150235.

20. Farrand, K.J., Dickgreber, N., Stoitzner, P., Ronchese, F., Petersen, T.R., and Hermans, I.F. (2009). Langerin+ CD8alpha+ dendritic cells are critical for cross-priming and IL-12 production in response to systemic antigens. J. Immunol. *183*, 7732–7742. https://doi.org/10.4049/jimmunol.0902707.

21. Lehmann, C.H.K., Baranska, A., Heidkamp, G.F., Heger, L., Neubert, K., Lühr, J.J., Hoffmann, A., Reimer, K.C., Brückner, C., Beck, S., et al. (2017). DC subset-specific induction of T cell responses upon antigen uptake via Fcgamma receptors in vivo. J. Exp. Med. *214*, 1509–1528. https://doi.org/10.1084/jem.20160951.

22. Martinez-Lopez, M., Iborra, S., Conde-Garrosa, R., and Sancho, D. (2015). Batf3-dependent CD103+ dendritic cells are major producers of IL-12 that drive local Th1 immunity against Leishmania major infection in mice. Eur. J. Immunol. *45*, 119–129. https://doi.org/10.1002/eji.201444651.

23. Sancho, D., Joffre, O.P., Keller, A.M., Rogers, N.C., Martínez, D., Hernanz-Falcón, P., Rosewell, I., and Reis e Sousa, C. (2009). Identification of a dendritic cell receptor that couples sensing of necrosis to immunity. Nature *458*, 899–903. https://doi.org/10.1038/nature07750.

24. Theisen, D.J., Davidson, J.T., 4th, Briseño, C.G., Gargaro, M., Lauron, E.J., Wang, Q., Desai, P., Durai, V., Bagadia, P., Brickner, J.R., et al. (2018). WDFY4 is required for cross-presentation in response to viral and tumor antigens. Science *362*, 694–699. https://doi.org/10.1126/science.aat5030.

25. Heger, L., Amon, L., Lehmann, C.H.K., Baranska, A., Heidkamp, G.F., and Dudziak, D. (2023). Functional Specialization of Dendritic Cell Subsets. In Encyclopedia of Cell Biology, R.A. Bradshaw, G.W. Hart, and P.D. Stahl, eds. (Academic Press), pp. 446–471. https://doi.org/10.1016/b978-0-12-821618-7.00257-1.

26. Heidkamp, G.F., Lehmann, C.H.K., Heger, L., Baransk, A., Hoffmann, A., Lühr, J., and Dudziak, D. (2016). Functional Specialization of Dendritic Cell Subsets. In Encyclopedia of Cell Biology, R.A. Bradshaw and P.D. Stahl, eds. (Academic Press), pp. 588–604. https://doi.org/10.1016/b978-0-12-394447-4.30076-1.

27. Chopin, M., Lun, A.T., Zhan, Y., Schreuder, J., Coughlan, H., D'Amico, A., Mielke, L.A., Almeida, F.F., Kueh, A.J., Dickins, R.A., et al. (2019). Transcription Factor PU.1 Promotes Conventional Dendritic Cell Identity and Function via Induction of Transcriptional Regulator DC-SCRIPT. Immunity *50*, 77–90.e5. https://doi.org/10.1016/j.immuni.2018.11.010.

28. Grajales-Reyes, G.E., Iwata, A., Albring, J., Wu, X., Tussiwand, R., Kc, W., Kretzer, N.M., Briseño, C.G., Durai, V., Bagadia, P., et al. (2015). Batf3 maintains autoactivation of Irf8 for commitment of a CD8alpha(+) conventional DC clonogenic progenitor. Nat. Immunol. *16*, 708–717. https://doi.org/10.1038/ni.3197.

29. Hildner, K., Edelson, B.T., Purtha, W.E., Diamond, M., Matsushita, H., Kohyama, M., Calderon, B., Schraml, B.U., Unanue, E.R., Diamond, M.S., et al. (2008). Batf3 deficiency reveals a critical role for CD8alpha+ dendritic cells in cytotoxic T cell immunity. Science *322*, 1097–1100. https://doi.org/10.1126/science.1164206.

30. Lau, C.M., Tiniakou, I., Perez, O.A., Kirkling, M.E., Yap, G.S., Hock, H., and Reizis, B. (2018). Transcription factor Etv6 regulates functional differentiation of cross-presenting classical dendritic cells. J. Exp. Med. *215*, 2265–2278. https://doi.org/10.1084/jem.20172323.

31. Murphy, T.L., Grajales-Reyes, G.E., Wu, X., Tussiwand, R., Briseño, C.G., Iwata, A., Kretzer, N.M., Durai, V., and Murphy, K.M. (2016). Transcriptional Control of Dendritic Cell Development. Annu. Rev. Immunol. *34*, 93–119. https://doi.org/10.1146/annurev-immunol-032713-120204.

32. Zhang, S., Coughlan, H.D., Ashayeripanah, M., Seizova, S., Kueh, A.J., Brown, D.V., Cao, W., Jacquelot, N., D'Amico, A., Lew, A.M., et al. (2021). Type 1 conventional dendritic cell fate and function are controlled by DC-SCRIPT. Sci. Immunol. *6*, eabf4432. https://doi.org/10.1126/sciimmunol.abf4432.

33. Gao, Y., Nish, S.A., Jiang, R., Hou, L., Licona-Limón, P., Weinstein, J.S., Zhao, H., and Medzhitov, R. (2013). Control of T helper 2 responses by transcription factor IRF4-dependent dendritic cells. Immunity *39*, 722–732. https://doi.org/10.1016/j.immuni.2013.08.028.

34. Kim, T.G., Kim, S.H., Park, J., Choi, W., Sohn, M., Na, H.Y., Lee, M., Lee, J.W., Kim, S.M., Kim, D.Y., et al. (2018). Skin-Specific CD301b(+) Dermal Dendritic Cells Drive IL-17-Mediated Psoriasis-Like Immune Response in Mice. J. Invest. Dermatol. *138*, 844–853. https://doi.org/10.1016/j.jid.2017.11.003.

35. Kumamoto, Y., Linehan, M., Weinstein, J.S., Laidlaw, B.J., Craft, J.E., and Iwasaki, A. (2013). CD301b(+) dermal dendritic cells drive T helper 2 cell-mediated immunity. Immunity *39*, 733–743. https://doi.org/10.1016/j.immuni.2013.08.029.

36. Lewis, K.L., Caton, M.L., Bogunovic, M., Greter, M., Grajkowska, L.T., Ng, D., Klinakis, A., Charo, I.F., Jung, S., Gommerman, J.L., et al. (2011). Notch2 receptor signaling controls functional differentiation of dendritic cells in the spleen and intestine. Immunity *35*, 780–791. https://doi.org/10.1016/j.immuni.2011.08.013.

37. Satpathy, A.T., Briseño, C.G., Lee, J.S., Ng, D., Manieri, N.A., Kc, W., Wu, X., Thomas, S.R., Lee, W.L., Turkoz, M., et al. (2013). Notch2-dependent classical dendritic cells orchestrate intestinal immunity to attaching-and-effacing bacterial pathogens. Nat. Immunol. *14*, 937–948. https://doi.org/10.1038/ni.2679.

38. Schlitzer, A., McGovern, N., Teo, P., Zelante, T., Atarashi, K., Low, D., Ho, A.W.S., See, P., Shin, A., Wasan, P.S., et al. (2013). IRF4 transcription factor-dependent CD11b+ dendritic cells in human and mouse control mucosal IL-17 cytokine responses. Immunity *38*, 970–983. https://doi.org/10.1016/j.immuni.2013.04.011.

39. Tussiwand, R., Everts, B., Grajales-Reyes, G.E., Kretzer, N.M., Iwata, A., Bagaitkar, J., Wu, X., Wong, R., Anderson, D.A., Murphy, T.L., et al. (2015). Klf4 expression in conventional dendritic cells is required for T helper 2 cell responses. Immunity *42*, 916–928. https://doi.org/10.1016/j.immuni.2015.04.017.

40. Bajana, S., Roach, K., Turner, S., Paul, J., and Kovats, S. (2012). IRF4 promotes cutaneous dendritic cell migration to lymph nodes during homeostasis and inflammation. J. Immunol. *189*, 3368–3377. https://doi.org/10.4049/jimmunol.1102613.

41. Caton, M.L., Smith-Raska, M.R., and Reizis, B. (2007). Notch-RBP-J signaling controls the homeostasis of CD8- dendritic cells in the spleen. J. Exp. Med. *204*, 1653–1664. https://doi.org/10.1084/jem.20062648.

42. Liu, T.T., Kim, S., Desai, P., Kim, D.H., Huang, X., Ferris, S.T., Wu, R., Ou, F., Egawa, T., Van Dyken, S.J., et al. (2022). Ablation of cDC2 development by triple mutations within the Zeb2 enhancer. Nature *607*, 142–148. https://doi.org/10.1038/s41586-022-04866-z.

43. Scott, C.L., Soen, B., Martens, L., Skrypek, N., Saelens, W., Taminau, J., Blancke, G., Van Isterdael, G., Huylebroeck, D., Haigh, J., et al. (2016). The transcription factor Zeb2 regulates development of conventional and plasmacytoid DCs by repressing Id2. J. Exp. Med. *213*, 897–911. https://doi.org/10.1084/jem.20151715.

44. Brown, C.C., Gudjonson, H., Pritykin, Y., Deep, D., Lavallée, V.P., Mendoza, A., Fromme, R., Mazutis, L., Ariyan, C., Leslie, C., et al. (2019). Transcriptional Basis of Mouse and Human Dendritic Cell Heterogeneity. Cell *179*, 846–863.e24. https://doi.org/10.1016/j.cell.2019.09.035.

45. Heger, L., Amon, L., Lehmann, C.H.K., and Dudziak, D. (2021). Systems Immunology Approaches for Understanding of Primary Dendritic Cell Subpopulations in the Past, Present and Future. In Systems Medicine, O. Wolkenhauer, ed. (Academic Press), pp. 501–510. https://doi.org/10.1016/b978-0-12-801238-3.11609-5.

46. Kabashima, K., Banks, T.A., Ansel, K.M., Lu, T.T., Ware, C.F., and Cyster, J.G. (2005). Intrinsic lymphotoxin-beta receptor requirement for homeostasis of lymphoid tissue dendritic cells. Immunity *22*, 439–450. https://doi.org/10.1016/j.immuni.2005.02.007.

47. Minutti, C.M., Piot, C., Pereira da Costa, M., Chakravarty, P., Rogers, N., Huerga Encabo, H., Cardoso, A., Loong, J., Bessou, G., Mionnet, C., et al. (2024). Distinct ontogenetic lineages dictate cDC2 heterogeneity. Nat. Immunol. *25*, 448–461. https://doi.org/10.1038/s41590-024-01745-9.

48. Narasimhan, H., Richter, M.L., Shakiba, R., Papaioannou, N.E., Stehle, C., Ravi Rengarajan, K., Ulmert, I., Kendirli, A., de la Rosa, C., Kuo, P.Y., et al. (2025). RORgammat-expressing dendritic cells are functionally versatile and evolutionarily conserved antigen-presenting cells. Proc. Natl. Acad. Sci. USA *122*, e2417308122. https://doi.org/10.1073/pnas.2417308122.

49. Papaioannou, N.E., Salei, N., Rambichler, S., Ravi, K., Popovic, J., Küntzel, V., Lehmann, C.H.K., Fiancette, R., Salvermoser, J., Gajdasik, D.W., et al. (2021). Environmental signals rather than layered ontogeny imprint the function of type 2 conventional dendritic cells in young and adult mice. Nat. Commun. *12*, 464. https://doi.org/10.1038/s41467-020-20659-2.

50. Rodrigues, P.F., Trsan, T., Cvijetic, G., Khantakova, D., Panda, S.K., Liu, Z., Ginhoux, F., Cella, M., and Colonna, M. (2024). Progenitors of distinct lineages shape the diversity of mature type 2 conventional dendritic cells. Immunity *57*, 1567–1585.e5. https://doi.org/10.1016/j.immuni.2024.05.007.

51. Satpathy, A.T., Kc, W., Albring, J.C., Edelson, B.T., Kretzer, N.M., Bhattacharya, D., Murphy, T.L., and Murphy, K.M. (2012). Zbtb46 expression distinguishes classical dendritic cells and their committed progenitors from other immune lineages. J. Exp. Med. *209*, 1135–1152. https://doi.org/10.1084/jem.20120030.

52. Vanderkerken, M., Baptista, A.P., De Giovanni, M., Fukuyama, S., Browaeys, R., Scott, C.L., Norris, P.S., Eberl, G., Di Santo, J.P., Vivier, E., et al. (2021). ILC3s control splenic cDC homeostasis via lymphotoxin signaling. J. Exp. Med. *218*, e20190835. https://doi.org/10.1084/jem.20190835.

53. Vremec, D., Pooley, J., Hochrein, H., Wu, L., and Shortman, K. (2000). CD4 and CD8 expression by dendritic cell subtypes in mouse thymus and spleen. J. Immunol. *164*, 2978–2986. https://doi.org/10.4049/jimmunol.164.6.2978.

54. Wu, X., Briseño, C.G., Durai, V., Albring, J.C., Haldar, M., Bagadia, P., Kim, K.W., Randolph, G.J., Murphy, T.L., and Murphy, K.M. (2016). Mafb lineage tracing to distinguish macrophages from other immune lineages reveals dual identity of Langerhans cells. J. Exp. Med. *213*, 2553–2565. https://doi.org/10.1084/jem.20160600.

55. Bar-On, L., Birnberg, T., Lewis, K.L., Edelson, B.T., Bruder, D., Hildner, K., Buer, J., Murphy, K.M., Reizis, B., and Jung, S. (2010). CX3CR1+ CD8alpha+ dendritic cells are a steady-state population related to plasmacytoid dendritic cells. Proc. Natl. Acad. Sci. USA *107*, 14745–14750. https://doi.org/10.1073/pnas.1001562107.

56. Lutz, K., Musumeci, A., Sie, C., Dursun, E., Winheim, E., Bagnoli, J., Ziegenhain, C., Rausch, L., Bergen, V., Luecken, M.D., et al. (2022). Ly6D(+)Siglec-H(+) precursors contribute to conventional dendritic cells via a Zbtb46(+)Ly6D(+) intermediary stage. Nat. Commun. *13*, 3456. https://doi.org/10.1038/s41467-022-31054-4.

57. Rodrigues, P.F., Kouklas, A., Cvijetic, G., Bouladoux, N., Mitrovic, M., Desai, J.V., Lima-Junior, D.S., Lionakis, M.S., Belkaid, Y., Ivanek, R., and Tussiwand, R. (2023). pDC-like cells are pre-DC2 and require KLF4 to control homeostatic CD4 T cells. Sci. Immunol. *8*, eadd4132. https://doi.org/10.1126/sciimmunol.add4132.

58. Sulczewski, F.B., Maqueda-Alfaro, R.A., Alcántara-Hernández, M., Perez, O.A., Saravanan, S., Yun, T.J., Seong, D., Arroyo Hornero, R., Raquer-McKay, H.M., Esteva, E., et al. (2023). Transitional dendritic cells are distinct from conventional DC2 precursors and mediate proinflammatory antiviral responses. Nat. Immunol. *24*, 1265–1280. https://doi.org/10.1038/s41590-023-01545-7.

59. Zhu, Y., Cai, P., Li, Z., Zhang, S., Kong, W.T., Wang, H., Gao, F., Zeng, Y., Qian, J., Su, B., et al. (2025). Transcription factors TCF4 and KLF4 respectively control the development of the DC2A and DC2B lineages. Nat. Immunol. *26*, 1275–1286. https://doi.org/10.1038/s41590-025-02208-5.

60. Liu, Z., Wang, H., Li, Z., Dress, R.J., Zhu, Y., Zhang, S., De Feo, D., Kong, W.T., Cai, P., Shin, A., et al. (2023). Dendritic cell type 3 arises from Ly6C(+) monocyte-dendritic cell progenitors. Immunity *56*, 1761–1777.e6. https://doi.org/10.1016/j.immuni.2023.07.001.

61. Mayer, C.T., Ghorbani, P., Nandan, A., Dudek, M., Arnold-Schrauf, C., Hesse, C., Berod, L., Stüve, P., Puttur, F., Merad, M., and Sparwasser, T. (2014). Selective and efficient generation of functional Batf3-dependent CD103+ dendritic cells from mouse bone marrow. Blood *124*, 3081–3091. https://doi.org/10.1182/blood-2013-12-545772.

62. Sathe, P., Pooley, J., Vremec, D., Mintern, J., Jin, J.O., Wu, L., Kwak, J.Y., Villadangos, J.A., and Shortman, K. (2011). The acquisition of antigen cross-presentation function by newly formed dendritic cells. J. Immunol. *186*, 5184–5192. https://doi.org/10.4049/jimmunol.1002683.

63. Helft, J., Böttcher, J., Chakravarty, P., Zelenay, S., Huotari, J., Schraml, B.U., Goubau, D., and Reis e Sousa, C. (2015). GM-CSF Mouse Bone Marrow Cultures Comprise a Heterogeneous Population of CD11c(+) MHCII(+) Macrophages and Dendritic Cells. Immunity *42*, 1197–1211. https://doi.org/10.1016/j.immuni.2015.05.018.

64. Hamilton, J.A. (2020). GM-CSF in inflammation. J. Exp. Med. *217*, e20190945. https://doi.org/10.1084/jem.20190945.

65. Becher, B., Tugues, S., and Greter, M. (2016). GM-CSF: From Growth Factor to Central Mediator of Tissue Inflammation. Immunity *45*, 963–973. https://doi.org/10.1016/j.immuni.2016.10.026.

66. Dress, R.J., Dutertre, C.A., Giladi, A., Schlitzer, A., Low, I., Shadan, N.B., Tay, A., Lum, J., Kairi, M.F.B.M., Hwang, Y.Y., et al. (2019). Plasmacytoid dendritic cells develop from Ly6D(+) lymphoid progenitors distinct from the myeloid lineage. Nat. Immunol. *20*, 852–864. https://doi.org/10.1038/s41590-019-0420-3.

67. Salei, N., Rambichler, S., Salvermoser, J., Papaioannou, N.E., Schuchert, R., Pakalniškytė, D., Li, N., Marschner, J.A., Lichtnekert, J., Stremmel, C., et al. (2020). The Kidney Contains Ontogenetically Distinct Dendritic Cell and Macrophage Subtypes throughout Development That Differ in Their Inflammatory Properties. J. Am. Soc. Nephrol. *31*, 257–278. https://doi.org/10.1681/ASN.201904041.

68. Menezes, S., Melandri, D., Anselmi, G., Perchet, T., Loschko, J., Dubrot, J., Patel, R., Gautier, E.L., Hugues, S., Longhi, M.P., et al. (2016). The Heterogeneity of Ly6C(hi) Monocytes Controls Their Differentiation into iNOS(+) Macrophages or Monocyte-Derived Dendritic Cells. Immunity *45*, 1205–1218. https://doi.org/10.1016/j.immuni.2016.12.001.

69. Kelly, B.L., and Locksley, R.M. (2000). Coordinate regulation of the IL-4, IL-13, and IL-5 cytokine cluster in Th2 clones revealed by allelic expression patterns. J. Immunol. *165*, 2982–2986. https://doi.org/10.4049/jimmunol.165.6.2982.

70. McKenzie, A.N., Li, X., Largaespada, D.A., Sato, A., Kaneda, A., Zurawski, S.M., Doyle, E.L., Milatovich, A., Francke, U., Copeland, N.G., et al.

(1993). Structural comparison and chromosomal localization of the human and mouse IL-13 genes. J. Immunol. *150*, 5436–5444.

71. Inaba, K., Inaba, M., Romani, N., Aya, H., Deguchi, M., Ikehara, S., Muramatsu, S., and Steinman, R.M. (1992). Generation of large numbers of dendritic cells from mouse bone marrow cultures supplemented with granulocyte/macrophage colony-stimulating factor. J. Exp. Med. *176*, 1693–1702. https://doi.org/10.1084/jem.176.6.1693.
72. Lutz, M.B., Ali, S., Audiger, C., Autenrieth, S.E., Berod, L., Bigley, V., Cyran, L., Dalod, M., Dörrie, J., Dudziak, D., et al. (2023). Guidelines for mouse and human DC generation. Eur. J. Immunol. *53*, e2249816. https://doi.org/10.1002/eji.202249816.
73. Lutz, M.B., Kukutsch, N., Ogilvie, A.L., Rössner, S., Koch, F., Romani, N., and Schuler, G. (1999). An advanced culture method for generating large quantities of highly pure dendritic cells from mouse bone marrow. J. Immunol. Methods *223*, 77–92. https://doi.org/10.1016/s0022-1759(98)00204-x.
74. Becher, B., Schlitzer, A., Chen, J., Mair, F., Sumatoh, H.R., Teng, K.W.W., Low, D., Ruedl, C., Riccardi-Castagnoli, P., Poidinger, M., et al. (2014). High-dimensional analysis of the murine myeloid cell system. Nat. Immunol. *15*, 1181–1189. https://doi.org/10.1038/ni.3006.
75. Bogunovic, M., Ginhoux, F., Helft, J., Shang, L., Hashimoto, D., Greter, M., Liu, K., Jakubzick, C., Ingersoll, M.A., Leboeuf, M., et al. (2009). Origin of the lamina propria dendritic cell network. Immunity *31*, 513–525. https://doi.org/10.1016/j.immuni.2009.08.010.
76. Greter, M., Helft, J., Chow, A., Hashimoto, D., Mortha, A., Agudo-Cantero, J., Bogunovic, M., Gautier, E.L., Miller, J., Leboeuf, M., et al. (2012). GM-CSF controls nonlymphoid tissue dendritic cell homeostasis but is dispensable for the differentiation of inflammatory dendritic cells. Immunity *36*, 1031–1046. https://doi.org/10.1016/j.immuni.2012.03.027.
77. King, I.L., Kroenke, M.A., and Segal, B.M. (2010). GM-CSF-dependent, CD103+ dermal dendritic cells play a critical role in Th effector cell differentiation after subcutaneous immunization. J. Exp. Med. *207*, 953–961. https://doi.org/10.1084/jem.20091844.
78. Kingston, D., Schmid, M.A., Onai, N., Obata-Onai, A., Baumjohann, D., and Manz, M.G. (2009). The concerted action of GM-CSF and Flt3-ligand on in vivo dendritic cell homeostasis. Blood *114*, 835–843. https://doi.org/10.1182/blood-2009-02-206318.
79. Vremec, D., Lieschke, G.J., Dunn, A.R., Robb, L., Metcalf, D., and Shortman, K. (1997). The influence of granulocyte/macrophage colony-stimulating factor on dendritic cell levels in mouse lymphoid organs. Eur. J. Immunol. *27*, 40–44. https://doi.org/10.1002/eji.1830270107.
80. Leach, S.M., Gibbings, S.L., Tewari, A.D., Atif, S.M., Vestal, B., Danhorn, T., Janssen, W.J., Wager, T.D., and Jakubzick, C.V. (2020). Human and Mouse Transcriptome Profiling Identifies Cross-Species Homology in Pulmonary and Lymph Node Mononuclear Phagocytes. Cell Rep. *33*, 108337. https://doi.org/10.1016/j.celrep.2020.108337.
81. Granot, T., Senda, T., Carpenter, D.J., Matsuoka, N., Weiner, J., Gordon, C.L., Miron, M., Kumar, B.V., Griesemer, A., Ho, S.H., et al. (2017). Dendritic Cells Display Subset and Tissue-Specific Maturation Dynamics over Human Life. Immunity *46*, 504–515. https://doi.org/10.1016/j.immuni.2017.02.019.
82. Hamilton, J.A., and Anderson, G.P. (2004). GM-CSF Biology. Growth Factors *22*, 225–231. https://doi.org/10.1080/08977190412331279881.
83. Neubert, K., Lehmann, C.H.K., Heger, L., Baranska, A., Staedtler, A.M., Buchholz, V.R., Yamazaki, S., Heidkamp, G.F., Eissing, N., Zebroski, H., et al. (2014). Antigen delivery to CD11c+CD8- dendritic cells induces protective immune responses against experimental melanoma in mice in vivo. J. Immunol. *192*, 5830–5838. https://doi.org/10.4049/jimmunol.1300975.
84. Zhan, Y., Carrington, E.M., van Nieuwenhuijze, A., Bedoui, S., Seah, S., Xu, Y., Wang, N., Mintern, J.D., Villadangos, J.A., Wicks, I.P., and Lew, A.M. (2011). GM-CSF increases cross-presentation and CD103 expression by mouse CD8(+) spleen dendritic cells. Eur. J. Immunol. *41*, 2585–2595. https://doi.org/10.1002/eji.201141540.
85. Breed, E.R., Voboril, M., Ashby, K.M., Martinez, R.J., Qian, L., Wang, H., Salgado, O.C., O'Connor, C.H., and Hogquist, K.A. (2022). Type 2 cytokines in the thymus activate Sirpalpha(+) dendritic cells to promote clonal deletion. Nat. Immunol. *23*, 1042–1051. https://doi.org/10.1038/s41590-022-01218-x.
86. Cook, P.C., Brown, S.L., Houlder, E.L., Furlong-Silva, J., Conn, D.P., Colombo, S.A.P., Baker, S., Svedberg, F.R., Howell, G., Bertuzzi, M., et al. (2025). Mgl2(+) cDC2s coordinate fungal allergic airway type 2, but not type 17, inflammation in mice. Nat. Commun. *16*, 928. https://doi.org/10.1038/s41467-024-55663-3.
87. Weckel, A., Dhariwala, M.O., Ly, K., Tran, V.M., Ojewumi, O.T., Riggs, J.B., Gonzalez, J.R., Dwyer, L.R., Okoro, J.N., Leech, J.M., et al. (2023). Long-term tolerance to skin commensals is established neonatally through a specialized dendritic cell subgroup. Immunity *56*, 1239–1254.e7. https://doi.org/10.1016/j.immuni.2023.03.008.
88. Denda-Nagai, K., Aida, S., Saba, K., Suzuki, K., Moriyama, S., Oo-Puthinan, S., Tsuiji, M., Morikawa, A., Kumamoto, Y., Sugiura, D., et al. (2010). Distribution and function of macrophage galactose-type C-type lectin 2 (MGL2/CD301b): efficient uptake and presentation of glycosylated antigens by dendritic cells. J. Biol. Chem. *285*, 19193–19204. https://doi.org/10.1074/jbc.M110.113613.
89. Singh, S.K., Streng-Ouwehand, I., Litjens, M., Kalay, H., Saeland, E., and van Kooyk, Y. (2011). Tumour-associated glycan modifications of antigen enhance MGL2 dependent uptake and MHC class I restricted CD8 T cell responses. Int. J. Cancer *128*, 1371–1383. https://doi.org/10.1002/ijc.25458.
90. Singh, S.K., Streng-Ouwehand, I., Litjens, M., Weelij, D.R., García-Vallejo, J.J., van Vliet, S.J., Saeland, E., and van Kooyk, Y. (2009). Characterization of murine MGL1 and MGL2 C-type lectins: distinct glycan specificities and tumor binding properties. Mol. Immunol. *46*, 1240–1249. https://doi.org/10.1016/j.molimm.2008.11.021.
91. Izumi, G., Nakano, H., Nakano, K., Whitehead, G.S., Grimm, S.A., Fessler, M.B., Karmaus, P.W., and Cook, D.N. (2021). CD11b(+) lung dendritic cells at different stages of maturation induce Th17 or Th2 differentiation. Nat. Commun. *12*, 5029. https://doi.org/10.1038/s41467-021-25307-x.
92. Mayer, J.U., Hilligan, K.L., Chandler, J.S., Eccles, D.A., Old, S.I., Domingues, R.G., Yang, J., Webb, G.R., Munoz-Erazo, L., Hyde, E.J., et al. (2021). Homeostatic IL-13 in healthy skin directs dendritic cell differentiation to promote T(H)2 and inhibit T(H)17 cell polarization. Nat. Immunol. *22*, 1538–1550. https://doi.org/10.1038/s41590-021-01067-0.
93. Bick, F., Blanchetot, C., Lambrecht, B.N., and Schuijs, M.J. (2025). Targeting gammac family cytokines with biologics: current status and future prospects. mAbs *17*, 2468312. https://doi.org/10.1080/19420862.2025.2468312.
94. Dougan, M., Dranoff, G., and Dougan, S.K. (2019). GM-CSF, IL-3, and IL-5 Family of Cytokines: Regulators of Inflammation. Immunity *50*, 796–811. https://doi.org/10.1016/j.immuni.2019.03.022.
95. Huang, I.H., Chung, W.H., Wu, P.C., and Chen, C.B. (2022). JAK-STAT signaling pathway in the pathogenesis of atopic dermatitis: An updated review. Front. Immunol. *13*, 1068260. https://doi.org/10.3389/fimmu.2022.1068260.
96. van de Laar, L., Coffer, P.J., and Woltman, A.M. (2012). Regulation of dendritic cell development by GM-CSF: molecular control and implications for immune homeostasis and therapy. Blood *119*, 3383–3393. https://doi.org/10.1182/blood-2011-11-370130.
97. Vento-Tormo, R., Company, C., Rodríguez-Ubreva, J., de la Rica, L., Urquiza, J.M., Javierre, B.M., Sabarinathan, R., Luque, A., Esteller, M., Aran, J.M., et al. (2016). IL-4 orchestrates STAT6-mediated DNA demethylation leading to dendritic cell differentiation. Genome Biol. *17*, 4. https://doi.org/10.1186/s13059-015-0863-2.
98. Linehan, J.L., Dileepan, T., Kashem, S.W., Kaplan, D.H., Cleary, P., and Jenkins, M.K. (2015). Generation of Th17 cells in response to intranasal infection requires TGF-beta1 from dendritic cells and IL-6 from

CD301b+ dendritic cells. Proc. Natl. Acad. Sci. USA *112*, 12782–12787. https://doi.org/10.1073/pnas.1513532112.

99. Amon, L., Dudziak, D., Backer, R.A., Clausen, B.E., Gmeiner, C., Heger, L., Jacobi, L., Lehmann, C.H.K., Probst, H.C., Seichter, A., et al. (2023). Guidelines for DC preparation and flow cytometry analysis of mouse lymphohematopoietic tissues. Eur. J. Immunol. *53*, e2249893. https://doi.org/10.1002/eji.202249893.

100. McInnes, L., Healy, J., and Melville, J. (2018). Umap: Uniform manifold approximation and projection for dimension reduction. Preprint at arXiv. https://doi.org/10.48550/arXiv:1802.03426.

STAR★METHODS

KEY RESOURCES TABLE

REAGENT or RESOURCE	SOURCE	IDENTIFIER
Antibodies		
anti-mouse CD3ε Biotin (Clone 145-2C11)	BioLegend	#100304; RRID: AB_312669
anti-mouse CD3ε Biotin (Clone 145-2C11)	eBioscience	#13-0031-85; RRID: AB_466320
anti-mouse CD3ε BUV737 (Clone 17A2)	BD Biosciences	#612803; RRID: AB_2870130
anti-mouse CD3ε A647 (Clone 145-2C11)	BioLegend	#100322; RRID: AB_389322
anti-mouse CD4 A488 (Clone GK1.5)	BioLegend	#100423; RRID: AB_389302
anti-mouse CD4 APC-Fire750 (Clone RM4-5)	BioLegend	#100568; RRID: AB_2629699
anti-mouse CD4 FITC (Clone RM4-5)	BioLegend	#100510; RRID: AB_312713
anti-mouse CD5 A647 (Clone 53–7.3)	BioLegend	#100614; RRID: AB_2075301
anti-mouse CD8α A488 (Clone 53–6.7)	BioLegend	#100723; RRID: AB_389304
anti-mouse CD8α BV570 (Clone 53–6.7)	BioLegend	#100740; RRID: AB_2563055
anti-mouse CD8α FITC (Clone 53–6.7)	BioLegend	#100706; RRID: AB_312745
anti-mouse CD19 Biotin (Clone 6D5)	BioLegend	#115504; RRID: AB_313638
anti-mouse CD19 Biotin (Clone 1D3)	eBioscience	#13-0193-85; RRID: AB_657658
anti-mouse CD19 BUV737 (Clone 1D3)	BD Biosciences	#612781; RRID: AB_2870110
anti-mouse Ly6G Biotin (Clone 1A8)	BioLegend	#127604; RRID: AB_1186105
anti-mouse Ly6G FITC (Clone 1A8)	BD Biosciences	#551460; RRID: AB_394207
anti-mouse Ly6G PE-Cy5 (Clone 1A8)	BioLegend	#127672
anti-mouse Ly6A/E A647 (Clone E13–161.7)	BioLegend	#122518; RRID: AB_2143238
anti-mouse Ly6A/E PerCP-Cy5.5 (Clone E13–161.7)	BioLegend	#122524; RRID: AB_893617
anti-mouse Ter119 Biotin (Clone TER-119)	BioLegend	#116204; RRID: AB_313704
anti-mouse Ter119 PE-Cy5 (Clone TER-119)	BioLegend	#116210; RRID: AB_313711
anti-mouse CD90.2 Biotin (Clone 53–2.1)	BioLegend	#140314; RRID: AB_10643274
anti-mouse Siglec-H BUV737 (Clone 440c)	BD Biosciences	#748293; RRID: AB_2872719
anti-mouse Siglec-H FITC (Clone 551)	BioLegend	#129604; RRID: AB_1227760
anti-mouse Siglec-H PE (Clone 551)	BioLegend	#129606; RRID: AB_2189147
anti-mouse Siglec-H PE-Cy7 (clone eBio440c)	eBioscience	#25-0333-82; RRID: AB_2573342
anti-mouse NK1.1 BUV395 (Clone PK136)	BD Biosciences	#564144; RRID: AB_2738618
anti-mouse NK1.1 BUV395 (Clone PK136)	eBioscience	#363-5941-82; RRID: AB_2925297
anti-mouse CX3CR1 BV711 (Clone SA011F11)	BioLegend	#149031; RRID: AB_2565939
anti-mouse CX3CR1 BV785 (Clone SA011F11)	BioLegend	#149029; RRID: AB_2565938
anti-mouse CD317 BV650 (Clone 927)	BioLegend	#127019; RRID: AB_2562477
anti-mouse CD317 A647 (Clone 927)	BioLegend	#127014; RRID: AB_1953289
anti-mouse CD45 BV605 (Clone 30-F11)	BioLegend	#103140; RRID: AB_2562341
anti-mouse CD45.1 PE-Cy5 (Clone A20)	eBioscience	#15-0453-82; RRID: AB_468759
anti-mouse CD45.1 PE (Clone A20)	BioLegend	#110708; RRID: AB_313497
anti-mouse CD45.1 eFluor450 (Clone A20)	eBioscience	#48-0453-82; RRID: AB_1272189
anti-mouse CD45.2 BUV737 (Clone 104)	BD Biosciences	#612778; RRID: AB_2870107
anti-mouse CD45.2 A700 (Clone 104)	BioLegend	#109822; RRID: AB_493731

(*Continued on next page*)

Continued

REAGENT or RESOURCE	SOURCE	IDENTIFIER
anti-mouse CD49b Biotin (Clone DX5)	BioLegend	#108904; RRID: AB_313411
anti-mouse CD49b PE-Cy5 (Clone DX5)	eBioscience	#15-5971-82; RRID: AB_2573070
anti-mouse Ly6C BV570 (Clone HK1.4)	BioLegend	#128030; RRID: AB_2562617
anti-mouse Ly6C BV711 (Clone HK1.4)	BioLegend	#128037; RRID: AB_2562630
anti-mouse Ly6C APC-e780 (Clone HK1.4)	eBioscience	#47-5932-82; RRID: AB_2573992
anti-mouse Ly6C APC-e780 (Clone AL-21)	BD Biosciences	#561237; RRID: AB_10612017
anti-mouse MHC-II (I-A & I-E) V500 (Clone M5/114.15.2)	BD Biosciences	#562366; RRID: AB_11153488
anti-mouse H-2k^{b}/H-2D^{b} A647 (Clone 28-8-6)	BioLegend	#114612; RRID: AB_492931
anti-mouse TCR V alpha 2 PerCP-e710 (Clone B20.1)	eBioscience	#46-5812-80; RRID: AB_11039487
anti-mouse TCR V alpha 2 PE (Clone B20.1)	BioLegend	#127808; RRID: AB_1134183
anti-mouse Vβ 5.1, 5.2 T cell receptor BV421 (Clone MR9-4)	BD Biosciences	#742998; RRID: AB_2741196
anti-mouse/rat XCR1 BV421 (Clone ZET)	BioLegend	#148216; RRID: AB_2565230
anti-mouse/rat XCR1 APC (Clone ZET)	BioLegend	#148206; RRID: AB_2563932
anti-mouse/rat XCR1 FITC (Clone ZET)	BioLegend	#148210; RRID: AB_2564366
anti-mouse/rat XCR1 BV650 (Clone ZET)	BioLegend	#148220; RRID: AB_2566410
anti-mouse/rat XCR1 PE (Clone ZET)	BioLegend	#148204; RRID: AB_2563843
anti-mouse/rat XCR1 APC-Cy7 (Clone ZET)	BioLegend	#148224; RRID: AB_2783118
anti-mouse CD172a PerCP-e710 (Clone P84)	eBioscience	#46-1721-82; RRID: AB_10804639
anti-mouse CD172a BV605 (Clone P84)	BD Biosciences	#740390; RRID: AB_2740120
anti-mouse ESAM FITC (Clone 1G8)	BioLegend	#136205; RRID: AB_2044017
anti-mouse ESAM PE (Clone 1G8)	BioLegend	#136204; RRID: AB_1953301
anti-mouse ESAM A647 (Clone 1G8)	BD Biosciences	#567162; RRID: AB_2916479
anti-mouse ESAM PE-Cy7 (Clone 1G8)	BioLegend	#136212; RRID: AB_2860680
anti-mouse MerTK PE-Cy7 (Clone DS5MMER)	eBioscience	#25-5751-82; RRID: AB_2573466
anti-mouse MerTK PE (Clone DS5MMER)	eBioscience	#12-5751-82; RRID: AB_2572623
anti-mouse MerTK PE-Cy7 (Clone 2B10C42)	BioLegend	#151522
anti-mouse MerTK FITC (Clone 2B10C42)	BioLegend	#151504; RRID: AB_2617035
anti-mouse/human B220 PE-Cy5 (Clone RA3-6B2)	BioLegend	#103210; RRID: AB_312995
anti-mouse/human B220 PE (Clone RA3-6B2)	BioLegend	#103208; RRID: AB_312993
anti-mouse/human B220 Biotin (Clone RA3-6B2)	BioLegend	#103204; RRID: AB_312989
anti-mouse/human B220 BV650 (Clone RA3-6B2)	BioLegend	#103241; RRID: AB_11204069
anti-mouse CD11c PE-CF594 (Clone HL3)	BD Biosciences	#562454; RRID: AB_2737617
anti-mouse CD11c A647 (Clone N418)	BioLegend	#117312; RRID: AB_389328
anti-mouse CD11c A700 (Clone N418)	eBioscience	#56-0114-82; RRID: AB_493992
anti-mouse CD11c PE-eFluor610 (Clone N418)	eBioscience	#61-0114-82; RRID: AB_2574530
anti-mouse CD11c BV650 (Clone N418)	BioLegend	#117339; RRID: AB_2562414
anti-mouse CD11c FITC (Clone HL3)	BD Biosciences	#553801; RRID: AB_395060
anti-mouse CD123 PE (Clone 5B11)	BioLegend	#106005; RRID: AB_2124403

(*Continued on next page*)

Continued

REAGENT or RESOURCE	SOURCE	IDENTIFIER
anti-mouse CD124 APC (Clone I015F8)	BioLegend	#144808; RRID: AB_2750452
anti-mouse CD125 PE (Clone DIH37)	BioLegend	#153404; RRID: AB_2715829
anti-mouse CD131 PE (Clone JORO50)	BD Biosciences	#559920; RRID: AB_397374
anti-mouse CD132 APC (Clone TUGm2)	BioLegend	#132308; RRID: AB_10643576
anti-mouse CD133 BV421 (Clone 315-2C11)	BioLegend	#141213; RRID: AB_2566011
anti-mouse CD140a BV421 (Clone APA5)	BioLegend	#135923; RRID: AB_2814036
anti-mouse CD157 APC (Clone BP-3)	BioLegend	#140208; RRID: AB_10901172
anti-mouse CD183 BV421 (Clone CXCR3-173)	BD Biosciences	#562937; RRID: AB_2687551
anti-mouse CD196 A647 (Clone 140706)	BD Biosciences	#557976; RRID: AB_2228793
anti-mouse CD197 APC (Clone 4B12)	BioLegend	#120108; RRID: AB_389234
anti-mouse CD21/CD35 A647 (Clone 7E9)	BioLegend	#123424; RRID: AB_2629578
anti-mouse CD25 BV421 (Clone PC61)	BioLegend	#102043; RRID: AB_2562611
anti-mouse CD43 FITC (Clone S7)	BD Biosciences	#553270; RRID: AB_394747
anti-mouse CD103 APC-Cy7 (Clone 2E7)	BioLegend	#121432; RRID: AB_2566551
anti-mouse CD103 BV711 (Clone 2E7)	BioLegend	#121435
anti-mouse CD103 FITC (Clone 2E7)	BioLegend	#121420
anti-mouse CD103 PE (Clone 2E7)	eBioscience	#12-1031-83; RRID: AB_465800
anti-mouse CD31 BV421 (Clone 390)	BioLegend	#102424; RRID: AB_2650892
anti-mouse CD39 A647 (Clone Duha59)	BioLegend	#143808; RRID: AB_2563978
anti-mouse CD74 BV421 (Clone In-1)	BD Biosciences	#740057; RRID: AB_2739822
anti-mouse/human CD11b A700 (Clone M1/70)	BioLegend	#101222; RRID: AB_493705
anti-mouse/human CD11b Biotin (Clone M1/70)	BioLegend	#101204; RRID: AB_312787
anti-mouse EpCAM BUV737 (Clone G8.8)	BD Biosciences	#741818; RRID: AB_2871153
anti-mouse EpCAM PE (Clone G8.8)	BioLegend	#118206; RRID: AB_1134172
anti-mouse EpCAM PE-Cy7 (Clone G8.8)	BioLegend	#118216; RRID: AB_1236471
anti-mouse/human CD324 PE (Clone DECMA-1)	BioLegend	#147304; RRID: AB_2563040
anti-mouse CD368 PE (Clone 3A4/Clec4d)	BD Biosciences	#571181; RRID: AB_3686309
anti-mouse Clec12A APC (Clone 5D3/CLEC12A)	BioLegend	#143406; RRID: AB_2564265
anti-mouse Clec12A PE (Clone 5D3/CLEC12A)	BioLegend	#143404; RRID: AB_11126984
anti-mouse Clec12A BV421 (Clone 5D3/CLEC12A)	BD Biosciences	#564795; RRID: AB_2738955
anti-mouse CD64 A647 (Clone X54-5/7.1)	BD Biosciences	#558539; RRID: AB_647120
anti-mouse CD64 FITC (Clone X54-5/7.1)	BioLegend	#139316; RRID: AB_2566556
anti-mouse DEC205 A647 (Clone NLDC-145)	BioLegend	#138204; RRID: AB_2297115
anti-mouse Clec9A PE (Clone 7H11)	BioLegend	#143504; RRID: AB_11147953
anti-mouse Clec9A APC (Clone 7H11)	BioLegend	#143506; RRID: AB_2566380
anti-mouse/human Langerin PE (Clone 4C7)	BioLegend	#144204; RRID: AB_2561498
anti-mouse FceR1alpha PE (Clone MAR-1)	eBioscience	#12-5898-82; RRID: AB_466028
anti-mouse DCIR1 PE (Clone TKKT-1)	BD Biosciences	#566810; RRID: AB_2869880
anti-mouse DCIR2 A647 (Clone 33D1)	BioLegend	#124912; RRID: AB_1227623
anti-mouse DCAR2 PE (Clone 7D2D3)	BD Biosciences	#566882; RRID: AB_2869933

(*Continued on next page*)

Continued

REAGENT or RESOURCE	SOURCE	IDENTIFIER
anti-mouse DCIR4 PE (Clone MH7E7)	BD Biosciences	#567034; RRID: AB_2870015
anti-mouse Dectin-1 APC (Clone bg1fpj)	eBioscience	#17-5859-82; RRID: AB_2573232
anti-mouse CD301b A647 (Clone URA-1)	BioLegend	#146806; RRID: AB_2563388
anti-mouse CD301b PE-Dazzle594 (Clone URA-1)	BioLegend	#146816; RRID: AB_2566027
anti-mouse CD301b PE-Cy7 (Clone URA-1)	BioLegend	#146808; RRID: AB_2563390
anti-mouse CD301a PE (Clone MGL1)	BD Biosciences	#568900; RRID: AB_3684616
anti-mouse Clec2 PE (Clone 17D9/CLEC-2)	BioLegend	#146104; RRID: AB_2562382
anti-mouse BTLA A647 (Clone 6A6)	BioLegend	#139106; RRID: AB_10613297
anti-mouse TIM3 PE (Clone RMT3-23)	eBioscience	#12-5870-82; RRID: AB_465974
anti-mouse VISTA PE (Clone MIH64)	BD Biosciences	#566269; RRID: AB_2744494
anti-mouse PD-L1 APC (Clone 10F.9G2)	BioLegend	#124312; RRID: AB_10612741
anti-mouse PD-L2 APC (Clone TY25)	BioLegend	#107210; RRID: AB_2566345
anti-mouse CD51 PE (Clone RMV-7)	BioLegend	#104106; RRID: AB_2129493
anti-mouse Siglec-F BUV395 (Clone E50-2440)	BD Biosciences	#567600; RRID: AB_2916663
anti-mouse CD169 A488 (Clone 3D6.112)	BioLegend	#142419; RRID: AB_2566436
anti-mouse CD169 A647 (Clone 3D6.112)	BioLegend	#142408; RRID: AB_2563621
anti-mouse CD88 APC (Clone 20/70)	BioLegend	#135808; RRID: AB_10899415
anti-mouse CD88 A488 (Clone 20/70)	eBioscience	#53-0882-82; RRID: AB_2811859
anti-mouse CD88 RY586 (Clone 20/70)	BD Biosciences	#753587
anti-mouse CD88 BV605 (Clone 20/70)	BD Biosciences	#743771; RRID: AB_2741739
anti-mouse CD88 BV510 (Clone 20/70)	BD Biosciences	#743770; RRID: AB_2741738
anti-mouse CD88 PerCP-Cy5.5 (Clone 20/70)	BioLegend	#135813; RRID: AB_2750209
anti-mouse CD135 PE (Clone A2F10)	eBioscience	#12-1351-82; RRID: AB_465859
anti-mouse CD135 Biotin (Clone A2F10)	BioLegend	#135308; RRID: AB_1953267
anti-mouse CD135 PE-Cy5 (Clone A2F10)	BioLegend	#135312; RRID: AB_2263031
anti-mouse CD26 APC (Clone H194-112)	BioLegend	#137807; RRID: AB_10663403
anti-mouse CD209a PE (Clone MMD3)	BioLegend	#833004; RRID: AB_2721637
anti-mouse CD24 FITC (Clone M1/69)	BioLegend	#101806; RRID: AB_312839
anti-mouse CD115 PE (Clone W19330E)	BioLegend	#165203; RRID: AB_2910352
anti-mouse CD115 PE-Cy7 (Clone AFS98)	BioLegend	#135524; RRID: AB_2566460
anti-mouse CD116 Purified (Clone 698423)	Invitrogen	#MA5-23918; RRID: AB_2608189
anti-mouse CD117 BV605 (Clone 2B8)	BD Biosciences	#563146; RRID: AB_2738028
anti-mouse CD117 APC-Fire750 (Clone 2B8)	BioLegend	#105838; RRID: AB_2616739
anti-mouse F4/80 A647 (Clone BM8)	BioLegend	#123122; RRID: AB_893480
anti-mouse CD80 PE (Clone 16-10A1)	BioLegend	#104708; RRID: AB_313128
anti-mouse CD86 PE (Clone GL-1)	BioLegend	#105008; RRID: AB_313151
anti-mouse CD45RB APC-Cy7 (Clone C363-16A)	BioLegend	#103310; RRID: AB_528821
Purified anti-mouse MARCO (Clone ED31)	Serotec	#MCA1849
anti-mouse CCR2 BV421 (Clone SA203G11)	BioLegend	#150605; RRID: AB_2571913
anti-mouse CCR7 PE-Cy7 (Clone 4B12)	eBioscience	#25-1971-82; RRID: AB_469652
anti-mouse CCR9 FITC (Clone 9B1)	BioLegend	#129706; RRID: AB_1227483
anti-mouse CD34 BV421 (Clone SA376A4)	BioLegend	#152208; RRID: AB_2650766
anti-mouse CD40 PE (Clone 3/23)	BD Biosciences	#553791; RRID: AB_395055

(*Continued on next page*)

Continued

REAGENT or RESOURCE	SOURCE	IDENTIFIER
anti-mouse CD44 BUV395 (Clone IM7)	BD Biosciences	#740215; RRID: AB_2739963
anti-mouse CD62L BV605 (Clone MEL-14)	BioLegend	#104438; RRID: AB_2563058
anti-mouse CD70 APC (Clone FR70)	BioLegend	#104610; RRID: AB_2750465
anti-mouse CD137-L PE (Clone TKS-1)	BioLegend	#107105; RRID: AB_2256408
anti-mouse CD275 PE (Clone HK5.3)	eBioscience	#12-5985-82; RRID: AB_466094
anti-mouse CD281 BV421 (Clone TR23)	BD Biosciences	#565792; RRID: AB_2739357
anti-mouse/human CD282 A647 (Clone Qa16A01)	BioLegend	#153008; RRID: AB_2728208
anti-mouse CD283 APC (Clone 11F8)	BioLegend	#141906; RRID: AB_2561437
anti-mouse CD284 PE (Clone SA15-21)	BioLegend	#145404; RRID: AB_2561874
anti-mouse CD285 PE (Clone ACT5)	BioLegend	#148108
anti-mouse CD286 BV421 (Clone C1N2)	BD Biosciences	#566005; RRID: AB_2739454
anti-mouse CD287 PE (Clone A94B10)	BioLegend	#160004; RRID: AB_2876562
anti-mouse CD289 PE (Clone S18025A)	BioLegend	#159104
anti-mouse CD357 BV510 (Clone DTA-1)	BD Biosciences	#740192; RRID: AB_2739945
anti-mouse CD357-L PE (Clone MIH44)	BD Biosciences	#563541; RRID: AB_2738269
anti-mouse TCRbeta PE-Cy5 (Clone H57-597)	eBioscience	#15-5961-82; RRID: AB_468816
anti-human/mouse/rat ICOS A700 (Clone C398.4A)	BioLegend	#313528; RRID: AB_2566126
anti-mouse LAG-3 APC (Clone C9B7W)	eBioscience	#17-2231-82; RRID: AB_2573184
anti-mouse lymphotoxin beta receptor PE (Clone 5G11)	BioLegend	#134403; RRID: AB_1659180
anti-mouse Notch2 APC (Clone HMN2-35)	BioLegend	#130714; RRID: AB_2153642
anti-mouse OX40 BV711 (Clone OX-86)	BioLegend	#119421; RRID: AB_2687176
anti-mouse PD-1 eFluor450 (Clone J43)	eBioscience	#48-9985-82; RRID: AB_2574139
anti-mouse/human IRF4 A647 (Clone IRF4.3E4)	BioLegend	#646408; RRID: AB_2564047
anti-mouse/human IRF8 APC (Clone V3GYWCH)	eBioscience	#17-9852-82; RRID: AB_2573318
anti-mouse/human MAFB Purified (Clone BLR046F)	Bethyl Laboratories via Thermo Fisher	#A700-046; RRID: AB_2891845
anti-mouse ZBTB46 PE (Clone U4-1374)	BD Biosciences	#565832
Isotype recombinant monoclonal rabbit IgG A488 (RbNP15)	eBioscience	#53-4616-82; RRID: AB_2848433
Isotype rat IgG1,κ PE (Clone RTK2071)	BioLegend	#400408; RRID: AB_326514
Isotype rat IgG1,κ A647 (Clone RTK2071)	BioLegend	#400418
Isotype rat IgG1,κ A488 (Clone RTK2071)	BioLegend	#400417; RRID: AB_389319
Isotype rat IgG1,κ APC (Clone RTK2071)	BioLegend	#400412; RRID: AB_326518
Isotype rat IgG2a,κ PE (Clone RTK2758)	BioLegend	#400508; RRID: AB_326530
Isotype rat IgG2a,κ A488 (Clone RTK2758)	BioLegend	#400525; RRID: AB_2864283
Isotype rat IgG2a,κ APC (Clone RTK2758)	BioLegend	#400512; RRID: AB_2814702
Isotype rat IgG2a,κ A647 (Clone RTK2758)	BioLegend	#400526; RRID: AB_2864284
Isotype rat IgG2a,κ FITC (Clone RTK2758)	BioLegend	#400506; RRID: AB_2736919
Isotype rat IgG2a,λ A647 (Clone B39-4)	BD Biosciences	#564281; RRID: AB_2869559
Isotype rat IgG2b,κ APC (Clone RTK4530)	BioLegend	#400612; RRID: AB_326556
Isotype rat IgG2b,κ FITC (Clone A95-1)	BD Biosciences	#553988; RRID: AB_479619
Isotype rat IgG2b,κ A647 (Clone RTK4530)	BioLegend	#400626; RRID: AB_389343
Isotype rat IgG2b,κ PE (Clone RTK4530)	BioLegend	#400608; RRID: AB_326552

(*Continued on next page*)

Continued

REAGENT or RESOURCE	SOURCE	IDENTIFIER
Isotype mouse IgG1,κ A647 (Clone MOPC-21)	BioLegend	#400130; RRID: AB_2800436
Isotype mouse IgG1,κ PE (Clone MOPC-21)	BioLegend	#400112; RRID: AB_2847829
Isotype mouse IgG1,κ APC (Clone MOPC-21)	BioLegend	#400122; RRID: AB_326443
Isotype mouse IgG1,κ FITC (Clone MOPC-21)	BD Biosciences	#555909
Isotype mouse IgG1,κ BV421 (Clone MOPC-21)	BioLegend	#400158; RRID: AB_11150232
Isotype mouse IgG2a,κ PE (Clone MOPC-173)	BioLegend	#400212; RRID: AB_326460
Isotype mouse IgG2a,κ A647 (Clone MOPC-173)	BioLegend	#400234; RRID: AB_2864287
Isotype mouse IgG2b,κ APC (Clone MPC-11)	BioLegend	#400320
Isotype Armenian Hamster IgG A647 (Clone HKT888)	BioLegend	#400924; RRID: AB_2922967
Isotype Armenian Hamster IgG PE (Clone eBio299Arm)	eBioscience	#12-4888-83; RRID: AB_470074
Isotype Armenian Hamster IgG FITC (Clone HKT888)	BioLegend	#400906
Isotype Armenian Hamster IgG BV421 (Clone HKT888)	BioLegend	#400949
Purified anti-mouse CD16/32 (Clone 2.4G2)	BioXCell	#BE0307
Purified anti-mouse CD16.2 (Clone 9E9)	BioLegend	#149502; RRID: AB_2565302
anti-mouse CD16/CD32 BV650 (Clone AB93)	BD Biosciences	#751690; RRID: AB_2875675
anti-mouse CD16/CD32 FITC (Clone 93)	BioLegend	#101306; RRID: AB_312805
Annexin V A647	BioLegend	#640912
Streptavidin BV421	BioLegend	#405226
Streptavidin PE-Cy7	BioLegend	#405206
Streptavidin BUV496	BD Biosciences	#612961; RRID: AB_2870237
Chemicals, peptides, and recombinant proteins		
Collagenase Type IV	Worthington	#LS0004186
Deoxyribonuclease I (DNAse I)	Roche	#11284932001
Procaine hydrochloride	Sigma Aldrich	#P9879
Sodium chloride	Roth	#3957.1
Magnesium sulfate	Roth	#0261.1
Calcium chloride	Roth	#HN04.3
Ammonium chloride	Roth	#K298.1
Potassium hydrogen carbonate	Roth	#P748.1
Dulbecco's Phosphate Buffered Saline without calcium and magnesium	Sigma Aldrich	#D8537
Hank's Balanced Salt Solution (HBSS) without calcium and magnesium	Sigma Aldrich	#H6648
Minimum Essential Medium (MEM) alpha modification	Sigma Aldrich	#M8042
RPMI-1640	Sigma Aldrich	#R8758
Fetal Bovine Serum (FCS)	Sigma Aldrich	#F7524
Normal Rat Serum	STEMCELL	#13551
L-glutamine solution	Sigma Aldrich	#G7513

(*Continued on next page*)

Continued

REAGENT or RESOURCE	SOURCE	IDENTIFIER
sodium pyruvate solution	Sigma Aldrich	#S8636
Penicillin-Streptomycin solution	Sigma Aldrich	#P4333
beta-Mercaptoethanol 50mM in DPBS	PAN Biotech	#P07-05100
HEPES buffer solution (1M)	gibco	#15630-056
0.05% Trypsin:EDTA solution	gibco	#25300-054
0.25% Trypsin:EDTA solution	Sigma Aldrich	#T4049
Lympholyte-M	Cedarlane	#CL5035
EDTA UltraPure 0.5M, pH 8.0	Invitrogen	#15575-038
Bovine Serum Albumin (BSA; Albumin Fraction V)	Roth	#8076.3
4′,6-diamidino-2-phenylindole (DAPI)	AppliChem	#A4099
Mitomycin-C	PanReac Applichem	#A2190,0002
Recombinant mouse FMS-like tyrosine kinase 3 ligand (FLT3-L; carrier-free)	BioLegend	#550706
Mouse Granulocyte-macrophage colony-stimulating-factor (GM-CSF)	PeproTech Inc.	#315-03
Recombinant murine Interleukin-3	ImmunoTools	#12340033
Recombinant murine Interleukin-4	ImmunoTools	#12340043
Recombinant murine Interleukin-5	ImmunoTools	#12340053
Recombinant murine Interleukin-13	ImmunoTools	#12340133
$OVA_{323-339}$ peptide (I-Ad restricted OVA-epitope)	InvivoGen	#vac-isq
$OVA_{257-264}$ peptide (H-2kb restricted OVA-epitope)	InvivoGen	#vac-sin
soluble OVA (sOVA) [In-house LPS removal via Triton X-114]	Sigma Aldrich	#A2512
R848 (Resiquimod)	InvivoGen	#tlrl-r848-5
Pam3CSK4	InvivoGen	#tlrl-pms
Zymosan	InvivoGen	#tlrl-ZYN
Poly(I:C) High Molecular Weight	InvivoGen	#tlrl-pic
CRX-527	InvivoGen	#tlrl-CRX527
ODN 1826	InvivoGen	#tlrl-1826
Critical commercial assays		
True-Nuclear™ Transcription Factor Buffer Set	BioLegend	#424401
Annexin V Binding Buffer	BioLegend	#422201
BD Cytofix/Cytoperm™	BD Biosciences	#554714
Zeba™ Spin Desalting Columns 7k MWCO, 0.05mL	Thermo Scientific	#89882
Precision Count Beads™	BioLegend	#424902
Alexa Fluor™ A488 Labeling Kit	Invitrogen	#A20181
CellTrace™ CFSE Cell Proliferation Kit	Invitrogen	#C34554
CBA Assay LEGENDPlex 11-plex Custom Mouse Panel 829	BioLegend	#900001929
MojoSort™ Streptavidin Nanobeads	BioLegend	#480016
anti-mouse CD11c MicroBeads UltraPure	Miltenyi Biotec	#130-125-835
EasySep™ Mouse CD11c Positive Selection Kit II	STEMCELL	#18780A
EasySep™ Mouse $CD4^+$ T cell Isolation Kit	STEMCELL	#19852A
EasySep™ Mouse $CD8^+$ T cell Isolation Kit	STEMCELL	#19853A

(*Continued on next page*)

Continued

REAGENT or RESOURCE	SOURCE	IDENTIFIER
Experimental models: Cell lines		
Murine MS5 stromal cells	Kindly provided by Prof. Dr. Stella E. Autenrieth	–
Experimental models: Organisms/strains		
C57BL/6J wildtype mice	Charles River	#C57/BL6″J″
B6.SJL-Ptprc^{a}Pep3^{b}/BoyJ CD45.1^{+}	The Jackson Laboratory via Charles River	#002014; RRID: IMSR_JAX:002014
C57BL/6-Tg(TcraTcrb)1100Mjb/J	The Jackson Laboratory via Charles River	#003831; RRID: IMSR_JAX:003831
B6.Cg-Tg(TcraTcrb)425Cbn/J	The Jackson Laboratory via Charles River	#004194; RRID: IMSR_JAX:004194
B6.Cg-Tg(Itgax-cre)1-1Reiz/J	The Jackson Laboratory via Charles River (Kindly provided by Prof. Dr. Falk Nimmerjahn)	#008068; RRID: IMSR_JAX:008068
B6.129S-Csf2tm1Mlg/J	The Jackson Laboratory (Kindly provided by Prof. Dr. Kai Hildner)	#026812; RRID: IMSR_JAX:026812
B6J-Csf2ra^{em1IRC}	Kindly provided by Prof. Dr. Bart Lambrecht	Newly generated
B6.129S1-Irf4tm1Rdf/J	The Jackson Laboratory via Charles River (Kindly provided by Prof. Dr. Kai Hildner)	#009380; RRID: IMSR_JAX:009380
Software and algorithms		
DIVA V7.0	BD Biosciences	https://www.bdbiosciences.com/en-de/products/software/instrument-software/bd-facsdiva-software
FlowJo V10	BD Biosciences	https://www.bdbiosciences.com/en-de/products/software/flowjo-v10-software
Plugin UMAP V3.1 & V4.0.3	McInnes et al., ArXiv, 2019;	https://www.flowjo.com/exchange/#/plugin/profile?id=6
Plugin down sample V3.3.1	BD Biosciences	https://www.flowjo.com/exchange/#/plugin/profile?id=25
Office 2019	Microsoft	https://www.microsoft.com/de-de/
GraphPad Prism 9	Graphpad	https://www.graphpad.com/
CorelDRAW 2021	Alludo	https://www.coreldraw.com
Other		
GentleMACS^{TM} Dissociator	Miltenyi Biotec	#130-093-235
C-tubes	Miltenyi Biotec	#130-096-334
Flow cytometer	BD Biosciences	BD LSRFortessa SORP
Sorter	BD Biosciences	BD Aria II SORP
Sorter	BD Biosciences	BD Aria III
5 mL Polypropylene Round-bottom Tube, sterile, 12x75 mm	FALCON	#352063
5 mL Polystyrene Round-bottom Tube, with Cell-Strainer Cap, 12x75 mm	FALCON	#352235
LS columns	Miltenyi Biotec	#130-042-401
EasySep^{TM} Magnet “The Big Easy”	STEMCELL	#18001
QuadroMACS^{TM} Separator	Miltenyi Biotec	#130-091-051
Safety-Multifly needle	Sarstedt	# 85.1642.201

EXPERIMENTAL MODEL AND STUDY PARTICIPANT DETAILS

Mice

In this study, female C57BL/6J were purchased from Charles River. OT-I CD45.2 and OT-II CD45.2 were obtained on a C57BL/6 background from The Jackson Laboratory and back-crossed with B6.SJL-Ptprc^{a}Pep3^{b}/BoyJ CD45.1^{+} mice to generate OT-I CD45.1^{+} and OT-II CD45.1^{+} mice. Further, CD11c^{CRE}xIRF4$^{fl/fl}$ mice were generated by intercrossing B6.Cg-Tg(Itgax-cre)1-1Reiz/J (kindly provided by Prof. Dr. Falk Nimmerjahn) with B6.129S1-Irf4tm1Rdf/J (kindly provided by Prof. Dr. Kai Hildner) mice. B6.129S-Csf2tm1Mlg/J mice were provided by Prof. Dr. Kai Hildner. In general, mice utilized in experiments had an age range

between 7 and 24 weeks. Listed mice were housed at the Präklinisches Experimentelles Tierzentrum (PETZ) of the Friedrich-Alexander-Universität Erlangen-Nürnberg (FAU) under specific-pathogen free conditions according to FELASA guidelines. All experiments were performed in accordance to institutional and national guidelines (TS-6/12; TS-11/2022, TS34-2021 Med1).

CD11c^{CRE}xCSF2Ra$^{fl/fl}$ were generated by intercrossing B6.Cg-Tg(Itgax-cre)1-1Reiz/J (acquired from the Jackson Laboratory) with B6J-Csf2ra^{em1IRC} mice (newly generated by the Lambrecht laboratory). All animals were housed under specific-pathogen-free conditions at the animal facility of Ghent University. Mice were housed in individually ventilated cages in a controlled day-night cycle and given food and water *ad libitum*. All experiments were approved by the animal ethics committee at Ghent University and were in accordance with Belgian animal protection law.

Generation of B6J-Csf2ra^{em1IRC} mice

This allele was generated by the Transgenic Core Facility (TCF) of the Center for Inflammation Research (IRC) of VIB-UGent by electroporating Cas9 RNP complex with guide sequence 5′ TCCCCACCGCGCGGACAAAG 3’ and ssDNA oligo 5′ AGGCCACA GGCAGGCAGGGCGACCCCCGATCCCCTCGACCGCCTCCCCACCGCGCGGACAggatccataacttcgtatagcatacattatacgaagttatAAG CGGGTCCACATATAAGCAAAGATTCACGGGGAATCAATAGGATAACGTCACCAAGAG 3’ containing a *loxP* site, immediately preceeded by a BamHI site to introduce a *loxP* site upstream of exon 2 (ENSMUSE00000640246) of the Csf2ra gene (ENSMU SG00000059326) in C57BL/6J embryos. The *loxP* + BamHI integrated after base position chr19:61216027. A second *loxP* site downstream of exon 2 was introduced by electroporating Cas9 RNP complex with guide sequence 5′ AAAAAGATCCTAGCTTCGGC 3’ and ssDNA oligo 5′ ACATTGAAAACTAATAGTAATAATAAATAAGTAATAATAAGAAAAAAAGATCCTAGCTTCgaattcataacttcgtataatgtatgct atacgaagttatGGCCGGGCTGTGTGGGTGGCAGAGGCAGGCAGGCAGGCAGAGAGGACCTCTGTGAGTTTG 3’ containing the downstream *loxP* site, immediately followed by an EcoRI site, in embryos already containing the upstream *loxP* site. The downstream *loxP* + EcoRI integrated after base position chr19:61212686. All base annotations are according to C57BL/6J genome assembly GRCm39.

Cell lines and cell culture

MS5 were cultured in Alpha MEM supplemented with 10% FCS, 2mM L-glutamine, 2mM sodium pyruvate, 100U/mL penicillin and 100μg/mL streptomycin at 37°C, 5% CO_2 and a relative humidity (rH) of 95%. Cultures were split before reaching complete confluence using 0.25% trypsin:EDTA solution. Before co-cultures, adherent MS5 stroma cells were treated with 10μg/mL mitomycin-C in MS5 culture medium for a total of 3h at 37°C (5%CO_2, 95%rH). Afterward, cells were washed twice with PBS, harvested using 0.05% trypsin:EDTA solution, filtered via a 100μm filter and washed three times with DC differentiation medium (RPMI-1640 without indicator supplemented with 10% FCS, 2mM L-glutamine, 100U/mL penicillin and 100μg/mL streptomycin, 10mM HEPES, and 50μM beta-mercaptoethanol) before co-culture.

METHOD DETAILS

Perfusion and tissue collection

To remove circulating blood cells from tissues, in particular from liver and lung, mice were sequentially perfused via the heart directly following euthanization using 3mL of sterile 0.9% (w/v) NaCl solution supplemented with 10% (w/v) dextran and 0.1% (w/v) procaine, 3mL of sterile 0.9% (w/v) NaCl solution, and finally 3mL of complete digestion buffer (Hank’s balanced salt solution supplemented with 2mM $CaCl_2$, 2mM $MgSO_4$, 210U/mL DNAse I (Roche) and 75U/mL Collagenase IV (Worthington)). Following perfusion, tissues were harvested.

Preparation of single-cell suspensions

If single-cell suspensions were subject for downstream procedures including enrichment and cell sorting procedures as well as differentiation and functional assays, single cell suspensions were prepared under a sterile bench using sterile buffers and aseptic techniques.

Single-cell suspensions were prepared as described previously.[11,12,99] In brief, spleens, thymi and lymph nodes were mechanically minced into small fragments and digested in 2mL of complete digestion buffer by incubation for 30 min at 37°C (5%CO_2, 95%rH). Afterward, tissue fragments were strained via a 100μm filter for singularization. In the case of splenic single cell suspensions, ACK lysis was performed for 5 min at room temperature (ACK lysis buffer 155mM NH_4Cl, 10mM $KHCO_3$, pH7.2), if single cell suspensions were employed for downstream flow cytometry, but not for enrichment and sorting procedures. Lysis was stopped using RPMI+2%FCS. Single-cell suspensions of spleens, lymph nodes, and thymi were passively filtered via a 40μm cell strainer and washed three times before downstream usage. Utilized buffers for washing are listed dependent on the downstream procedure in the table below.

Table 1. Overview preparation steps and employed buffers

Purpose	Tissue	Perfusion	Gradient	ACK lysis	Buffer after 40 μm filter
Direct flow cytometry	lung	yes	no	no	FACS buffer

(*Continued on next page*)

Table 1. *Continued*

Purpose	Tissue	Perfusion	Gradient	ACK lysis	Buffer after 40 μm filter
Direct flow cytometry	liver	yes	no	no	FACS buffer
Direct flow cytometry	spleen	yes[a]	no	yes	FACS buffer
Direct flow cytometry	lymph nodes	yes[a]	no	no	FACS buffer
Direct flow cytometry	thymus	yes[a]	no	no	FACS buffer
Direct flow cytometry	bone marrow	yes[a]	no	yes	FACS buffer
$CD4^+$ T cell enrichment (STEMCELL)	spleen	no	no	no	EasySep buffer
$CD8^+$ T cell enrichment (STEMCELL)	spleen	no	no	no	EasySep buffer
$CD11c^+$ enrichment (Miltenyi)	spleen	no	no	no	MACS buffer
$CD11c^+$ enrichment (STEMCELL)	spleen	no	no	no	EasySep buffer
Custom DC and monocyte enrichment	spleen	no	yes	no	MACS buffer
Custom pre-cDC enrichment	spleen/bone marrow	no	yes	no	MACS buffer

[a]For comparability, tissues were harvested from perfused mice, even though these tissues would not require perfusion per se. EasySep buffer, PBS + 2% FCS + 1 mM EDTA; FACS buffer, PBS + 2% FCS; and MACS buffer, PBS + 0.5% BSA + 2 mM EDTA, degassed.

Following isolation, lungs were transferred to C-tubes (Miltenyi) containing 3mL of complete digestion buffer and mechanically dissociated in the GentleMACS Dissociator (Miltenyi) by running program "m_lung_01.01" two times. Lungs were digested for 30 min in a water bath at 37°C while shaking, dissociated in the GentleMACS Dissociator using program "m_lung_02.01", and sequentially filtered via 100μm and 40μm cell strainers. Finally, cells were washed three times with FACS buffer (PBS+2%FCS) prior antibody staining.

Livers were mechanically minced and digested in 4mL/liver of complete digestion buffer for 45 min at 37°C (5% CO_2, 95%rH). After filtering via a 100μm filter, hepatocytes were sedimented at room temperature by two sequential centrifugations for 5 min at 10xg. The resulting supernatants were filtered via a 40μm cell strainer and washed three times with ice-cold FACS buffer before antibody staining.

For bone marrow single cell suspensions, tibia and femur of hindlegs were isolated, briefly dipped into 70% (v/v) EtOH and washed with PBS. Bone marrow cells were directly flushed out on a 100μm cell strainer using a 27G canula and RPMI+2%FCS. ACK lysis was performed for 5 min at room temperature, if single cell suspensions were subject to downstream flow cytometry. Lysis was stopped with RPMI+2%FCS, samples were filtered via 40μm cell strainers and washed three times before downstream usage. Utilized buffers for washing are listed dependent on the downstream procedure in the table below.

If bone marrow or splenic single cell suspensions were generated for the purpose of cell sorting, a density gradient centrifugation using Lympholyte-M lymphocyte separation medium (Cedarlane) was performed instead of ACK lysis. Therefore, $20x10^5$ nucleated cells were resuspended in 1mL of room temperature RPMI after filtering via 100μm and 40μm cell strainers and carefully overlaid in a 1:1 ratio onto room temperature Lympholyte-M. After centrifugation (1000xg, 20 min, room temperature, brake 1), leukocytes at the RPMI:Lympholyte-M interphase were harvested and washed three times with MACS buffer (PBS+0.5%-BSA+2mM EDTA).

Flow cytometry

Single cell suspensions were transferred to 96-well V-bottom plates for labeling with monoclonal antibodies (see key resource table). Samples were first stained for 20 min at 4°C in FACS buffer supplemented with biotinylated antibodies and the purified Fc blocking antibodies αFcγRIIB/III (Clone 2.4G2) and αFcγRIV (Clone 9E9). If FcγRIIB/III was used for active gating, fluorescently-labeled αFcγRIIB/III (Clone 93) was employed in combination with αFcγRIV (Clone 9E9) instead of purified αFcγRIIB/III (Clone 2.4G2). If FcγR expression was addressed, the 2.4G2 blocking antibody was not utilized if the expression of FcγRIIB, FcγRIII, or FcγRIV were analyzed, whereas blockade with 9E9 and 2.4G2 was not employed, if FcγRIV expression was assessed. Following the first staining, samples were washed three times with FACS buffer. In the case of biotin:streptavidin staining schemes, a second staining containing fluorescently-labeled antibodies and a streptavidin:dye-conjugate in FACS buffer were used for staining for 20 min at 4°C. After three rounds of washing, FACS buffer supplemented with DAPI (final concentration 100ng/mL) was added to the non-fixed samples directly before analysis at a BD LSR Fortessa SORP. Data was analyzed using DIVA and FlowJo V.10 software (BD). In staining schemes not employing a biotin:streptavidin detection scheme, Fc blockade and staining with fluorescently-labeled detection antibodies was performed within one staining step.

For the staining of nucleus and endosomal proteins, all incubations were performed at room temperature using exclusively room temperature centrifuges and solutions. Fixed cells were centrifuged at 900xg for 5 min. Intracellular staining of transcription factors was performed with the True-Nuclear Transcription Factor Buffer Set (BioLegend). After preparing 1xFix and 1xPerm/Wash solutions, cells resulting from the last washing step post extracellular staining were fixed for one hour in 150μL 1xFix solution. Subsequently, cells were washed twice with 1xPerm/Wash solution before resuspension in 75μL 1xPerm/Wash supplemented with 4% rat serum

and purified 9E9 (stock 0.5mg/mL; 1:400) and incubated for 10 min. Next, another 75μL 1xPerm/Wash containing fluorescently-labeled detection antibodies were mixed to the samples followed by incubation for one hour. Afterward, samples were washed three times with 1xPerm/Wash solution including two 5 min incubation steps before starting centrifugation. Finally, samples were washed and kept in ice-cold FACS buffer until analysis at a BD LSR Fortessa SORP. Intracellular staining of endosomal proteins was performed utilizing the BD Cytofix/Cytoperm Fixation/Permeabilization Kit (BD Biosciences). After fixation of samples in 50μL Fix solution for 30 min and two washing steps with 1xPerm/Wash solution, staining with fluorescently-labeled antibodies was performed for one hour in 50μL 1xPerm/Wash solution. After another three washes with 1xPerm/Wash, samples were finally washed and kept in ice-cold FACS buffer until analysis at a BD LSR Fortessa SORP.

Staining of Annexin V was performed after antibody-based surface marker staining in Annexin V Binding Buffer (BioLegend) for 15 min at room temperature. After washing, cells were analyzed in DAPI-containing Annexin V Binding Buffer at a BD LSR Fortessa SORP.

The αMafB and αCSF2RA antibodies utilized in this study were first cleared of preservatives such as NaN_3 via Zeba Spin Desalting Columns 7K MWCO (Thermo Scientific) and subsequently labeled in-house utilizing an Alexa Fluor 488 labeling kit (Thermo Fisher Scientific) according to the manufacturer's instructions.

Generation of cDCs from total bone marrow

For the generation and differentiation of cDCs, total bone marrow single cell suspensions were adjusted to a final concentration of $2x10^6$ cells/mL and seeded at day 0 in DC differentiation medium supplemented with either ±200ng/mL FLT3-ligand or ±100U/mL GM-CSF and further supplemented at day 4 with ±100U/mL GM-CSF, or different doses of recombinant murine IL-3, IL-4, IL-5, or IL-13 in dependence on the assay. Cultures were incubated at 37°C (5%CO_2, 95%rH). Finally, cells were harvested at day 6 for downstream use in flow cytometric analysis or cell sorting procedures.

Cell enrichment procedures and sorting

For CD11c enrichment of $CD11c^+$ cells from various tissues of C57BL/6J mice, anti-mouse CD11c MicroBeads UltraPure (Miltenyi) or the EasySep Mouse CD11c Positive Selection Kit II (STEMCELL) were employed. $CD4^+$ or $CD8^+$ T cells were negative enriched from splenic single cell suspensions of OT-II CD45.1 and OT-I CD45.1 mice using the EasySep Mouse $CD4^+$ T cell Isolation Kit or EasySep Mouse $CD8^+$ T cell Isolation Kit, respectively. All enrichment kits were used according to the manufacturer's instructions.

Splenic DCs of C57BL/6J mice were negative enriched following gradient centrifugation for sorting based on a custom enrichment protocol. Therefore, $1x10^8$ splenic single cells were Fc blocked (clone 2.4G2) in 250μL of MACS buffer for 5 min at 4°C. Next, a biotin-coupled antibody cocktail (αCD19, αB220, αCD90.2, αLy6G, αCD49b) in MACS buffer was added in a 1:1 ratio to the samples followed by labeling for 15 min at 4°C on a roller mixer. After three rounds of washing, $1x10^8$ cells were labeled with 10μL of MojoSort Streptavidin Nanobeads in 990μL MACS buffer for 15 min at 4°C on a roller mixer. Samples were washed, the concentration was adjusted to $1x10^8$ cells/mL and samples were placed into STEMCELL magnets (STEMCELL) for 5 min at room temperature. The unlabeled DC- and monocyte-containing supernatant was transferred to a fresh tube. Subsequently, $5x10^6$ cells were stained in 50μL of MACS buffer containing αCD3ε- and αTer119-Biotin antibodies for 10 min at 4°C, washed two times and finally stained in 50μL per $5x10^6$ cells of MACS buffer supplemented with fluorescently-labeled antibodies and a streptavidin:dye-conjugate. Following two washing steps, samples were sorted at a BD Aria II SORP and BD Aria III cell sorter into DC differentiation medium containing low-binding tubes (Corning).

For the untouched isolation and sorting of bone marrow and splenic pre-cDCs and pro-DC3s from C57BL/6J mice, a custom negative enrichment protocol was developed. For sorting pre-cDC1s and pre-cDC2s, $1x10^8$ cells were resuspended in 500μL MACS buffer containing Fc block 2.4G2 following gradient centrifugation. After 5 min of incubation on a roller mixer at 4°C, MACS buffer containing a biotin-labeled antibody cocktail for lineage depletion (bone marrow: αB220, αCD3ε, αCD19, αCD49b, αLy6G, αTer119, αCD11b; spleen: αB220, αCD3ε, αCD19, αCD49b, αLy6G, αTer119, αCD90.2) was added in a 1:1 ratio and samples were incubated for 15 min at 4°C on a roller mixer. For sorting of pre-cDC2s and pro-DC3s, samples were directly resuspended in the biotin-antibody cocktail supplemented with 2% normal rat serum allowing for αFcγRIIB/III antibody (clone 93) staining. Afterward, samples were washed three times, resuspended in 950μL MACS buffer supplemented with 50μL of MojoSort Streptavidin Nanobeads per $1x10^8$ cells and incubated for 15 min at 4°C on a roller mixer. After one wash, the concentration was adjusted to $1x10^8$ cells/mL and samples were placed into STEMCELL magnets (STEMCELL) for 5 min at room temperature. The unlabeled pre-cDC- and proDC3-containing supernatant was transferred to a fresh tube. A total of $1x10^6$ cells was stained in 50μL MACS buffer containing fluorescently-labeled antibodies for 15 min at 4°C on the roller mixer. Following two washing steps, samples were sorted at a BD Aria III cell sorter into DC differentiation medium containing low-binding tubes (Corning).

For the sorting of cDC subpopulations differentiated from total bone marrow *in vitro*, cells were harvested at day 6 of differentiation and stained for 15 min at 4°C in a mix containing Fc block 2.4G2 and biotinylated antibodies for lineage exclusion. Following washing, cells were stained for another 15 min at 4°C with fluorescently-labeled antibodies and a streptavidin:dye-conjugate. Following two washing steps, samples were sorted at a BD Aria II SORP and BD Aria III cell sorter into DC differentiation medium containing low-binding tubes (Corning).

Differentiation assays of cDCs on supporting bone marrow and splenocytes

Following sorting, 10,000 splenic cDC1s, Clec12A^{+}CD301b^{-} cDC2s, or ESAM^{+}CD301b^{-} cDC2 were cultured at 37°C (5%CO_2, 95%rH) in 100μL DC differentiation medium supplemented with 200ng/mL FLT3L ±100U/mL GM-CSF in 96-well U-bottom plates. Subsequently, cultures were analyzed for their CD103 and CD301b expression status via flow cytometry on day two post sorting.

For cultures of splenic DCs on bystander cells, a total of 5x10^{4} splenic CD45.2^{+} CD11c enriched DCs or sorted DCs were cultured at 37°C (5%CO_2, 95%rH) either alone or on a total of 5x10^{5} bone marrow- or spleen-derived CD45.1^{+} bystander cells (resulting from Lympholyte-M gradient centrifugation), or on 2.5x10^{4} MS5 stroma cells in DC differentiation medium ±200ng/mL FLT3L and ±100U/mL GM-CSF in 96-well F-bottom plates. After one and two days, the CD103 and CD301b expression status of contained DCs was analyzed via flow cytometry.

Differentiation assays of sorted pre-cDCs and pro-DC3s on bystander cells

Post sort, 5,000 pre-cDCs were differentiated at 37°C (5%CO_2, 95%rH) on top of an epithelial single cell layer formed by 25,000 Mitomycin-C treated MS5 cells in DC differentiation medium supplemented with 200ng/mL FLT3L ±100U/mL GM-CSF in 96-well F-bottom plates. Following a six-day incubation at 37°C (5% CO_2, 95%rH), DC output was analyzed via flow cytometry by utilizing a constant amount of Precision Count Beads (BioLegend) in a constant total volume per analyzed well. Precision Count Beads were detected during flow cytometry owing to their distinct SSC and FSC behavior distinguishing them from cells. For pre-cDC2s and pro-DC3s, cells were either cultured on Mitomycin-C treated MS5 cells or on CD45.1^{+} bystander bone marrow for two days before analysis via flow cytometry.

T cell:DC co-culture assays

Negative enriched CD4^{+} or CD8^{+} T cells from OT-II CD45.1 or OT-I CD45.1 mice were labeled with a final concentration of 15μM of Carboxyfluorescein succinimidyl ester (CFSE; Invitrogen) for 10 min at 37°C. After washing with RPMI+2%FCS, T cells were ready for downstream usage in co-culture systems. Following sorting of cDC subsets differentiated via FLT3-ligand ± GM-CSF from total bone marrow of C57BL/6J mice for a total of six days, sorted CD45.2^{+} cDC subsets were co-cultured with CFSE-labeled CD4^{+}CD45.1^{+} OT-II T cells or CD8^{+}CD45.1^{+} OT-I T cells at different ratios in DC differentiation medium in the presence or absence of 1μM $OVA_{(323-339)}$ or 1μM $OVA_{(257-264)}$ peptide (Invivogen), respectively. Additionally, DC:T cell co-cultures were performed in the presence or absence of 10μg/mL endotoxin-free soluble OVA (sOVA) ±1μg/mL ODN1826. After five days of incubation at 37°C (5%CO_2, 95%rH), co-cultures were analyzed via flow cytometry for T cell proliferation (CFSE dilution). All DC:T cell co-culture platforms were performed in 96-well U-bottom plates.

DC stimulation and cytokine measurements via CBA

To analyze cytokine production by DC subsets, a total of 20,000 sorted cells were seeded in 50μL of DC differentiation medium alone or 50μL of DC differentiation medium containing 1μg/mL of various TLR-ligands and subsequently incubated at 37°C (5%CO_2, 95%rH) for twelve hours in 96-well V-bottom plates before supernatants were harvested and stored at −80°C until performance of a cytometric bead array (CBA).

For the determination of cytokine concentrations in harvested supernatants, a customized 11-plex CBA kit (BioLegend) was used according to the manufacturer's instructions with minor modifications. In general, wells were loaded with 10μL assay buffer, 10μL standard solution or 10μL before the addition of 10μL antibody-immobilized bead cocktail. Samples were incubated at room temperature for two hours while shaking (500rpm). After two washing steps, samples were resuspended in 10μL of anti-cytokine antibody cocktail, incubated for one hour (500rpm), before addition of 10μL streptavidin-PE and a final incubation for 30 min (500rpm). Following two washing steps, samples were acquired at a BD LSR Fortessa SORP. Evaluation was performed using the online platform LEGENDplex Software (BioLegend). All cytokines shown were above the limit of detection (LOD).

QUANTIFICATION AND STATISTICAL ANALYSIS

Statistical analysis of usually interval scaled data was performed with GraphPad Prism V9. Gaussian distribution was assessed via the Saphiro-Wilk normality test to decide whether data is treated as parametric or non-parametric. If n was smaller than 6, a normal distribution was neglected by default and data was treated as non-parametric. To test for statistical significance of multi-group non-parametric unpaired data, the Kruskal Wallis test combined with Dunn's post hoc test was utilized, whereas paired data was assessed via the Friedman test. If only two groups of non-parametric unpaired or paired data were analyzed, a two-tailed test after Mann-Whitney or Wilcoxon test was utilized for rank comparison, respectively. To test for statistical significance of multi-group parametric data, one-way ANOVA followed by Tukey post hoc test was performed. Two-group comparisons of paired or unpaired parametric data was carried out by using paired or unpaired two-tailed t-tests. Detailed information on statistical testing, significance definitions in form of asterisks (*), plotted measures of central tendency and error, and biological and technical replica numbers are provided in the respective figure legend. If not mentioned otherwise, median ± interquartile range is displayed. $*p \leq 0.05$; $*p \leq 0.01$; $***p \leq 0.001$. Correlation analysis was done using two-tailed Spearman correlation for non-parametric data (confidence interval 95%).

Displayed heat maps and PCA analyses were performed in GraphPad Prism V9 following flow cytometry data normalization. Therefore, mean or median MFIs or ΔMFIs ($MFI_{staining}$-$MFI_{Isotype/FMO}$) calculated for different biological or technical replicas were normalized to the highest value on analyzed cell populations which was set to 100%. The described normalization was performed per antibody staining. To enable a direct judgment of the resulting relative expression (Percentage of maximum), the highest value utilized for normalization is displayed next to heat maps. Spider charts were plotted with Microsoft Excel 2019.

Flow cytometry data was acquired at a BD LSR Fortessa SORP and analyzed with FlowJo software. Unbiased clustering and dimensionality reduction approaches for flow cytometry data were performed based on publicly available FlowJo (BD Biosciences) plugins including UMAP.[100] Cell pools, cell numbers, and measured parameters utilized for clustering are summarized in the respective figure legends and/or associated main text. If not mentioned otherwise, UMAP was performed utilizing FSC-A, SSC-A, and parameters that were not employed for prior exclusion of lineage positive or dead cells.